Mon. Not. R. Astron. Soc. **000**, 000–000 (0000) Printed 25 January 2011 (MN LATEX style file v2.2)

The kinetic SZ tomography with spectroscopic redshift surveys

Jiawei Shao[1,2⋆], Pengjie Zhang[1]†, Weipeng Lin[1], Yipeng Jing[1], Jun Pan[3]
[1]*Key Laboratory for Research in Galaxies and Cosmology, Shanghai Astronomical Observatory, Nandan Road 80, Shanghai, 200030, China*
[2]*Graduate School of the Chinese Academy of Sciences, 19A, Yuquan Road, Beijing, China*
[3]*The Purple Mountain Observatory, 2 West Beijing Road, Nanjing 210008, China*

25 January 2011

ABSTRACT

The kinetic Sunyaev Zel'dovich effect (kSZ) effect is a potentially powerful probe to the missing baryons. However, the kSZ signal is overwhelmed by various contaminations and the cosmological application is hampered by loss of redshift information due to the projection effect. We propose a kSZ tomography method to alleviate these problems, with the aid of galaxy spectroscopic redshift surveys. We propose to estimate the large scale peculiar velocity through the 3D galaxy distribution, weigh it by the 3D galaxy density and adopt the product projected along the line of sight with a proper weighting as an estimator of the true kSZ temperature fluctuation Θ. Since the underlying directional dependence in the estimator $\hat{\Theta}$ closely resembles that in the true kSZ signal Θ, $\hat{\Theta}$ is tightly correlated with Θ. It thus avoids the problem of null correlation between the galaxy density and Θ, which prohibits the kSZ extraction through the usual density-CMB two-point cross correlation measurement. We thus propose to measure the kSZ signal through the $\hat{\Theta}$-Θ cross correlation. This approach has a number of advantages. (1) Due to the underlying directional dependence of $\hat{\Theta}$, it is uncorrelated with the primary CMB, the thermal SZ effect and astrophysical contaminations such as the dusty star forming galaxies. Thus the $\hat{\Theta}$-Θ cross correlation picks up the kSZ signal in the SZ survey with a clean manner. (2) With the aid of galaxy redshifts, the cross correlation recovers the redshift information of the kSZ signal and allows for more detailed investigation on missing baryons. (3) Since the galaxy surveys usually have high S/N, the S/N of the kSZ measurement through the $\hat{\Theta}$-Θ cross correlation can be significantly improved.

We test the proposed kSZ tomography against non-adiabatic and adiabatic hydrodynamical simulations. We confirm that $\hat{\Theta}$ is indeed tightly correlated with Θ at $k \lesssim 1h$/Mpc, although nonlinearities in the density and velocity fields and nonlinear redshift distortion do weaken the tightness of the $\hat{\Theta}$-Θ correlation. We further quantify the reconstruction noise in $\hat{\Theta}$ from galaxy distribution shot noise. Based on these results, we quantify the applicability of the proposed kSZ tomography for future surveys. We find that, in combination with the BigBOSS-N spectroscopic redshift survey, the PLANCK CMB experiment will be able to detect the kSZ with an overall significance of $\sim 50\sigma$ and further measure its redshift distribution at many redshift bins over $0 < z < 2$.

Key words: cosmology: observations – large-scale structure of Universe – cosmic microwave background

1 INTRODUCTION

Robust evidences from CMB and BBN show that the baryonic matter accounts for $\sim 4\%$ of the total matter and energy of the universe. However, only a fraction of this baryon budget has been detected in the local universe, either in the form of stars, interstellar medium (ISM) and intracluster medium (ICM) (refer to Fukugita & Peebles 2004, 2006 for census of the baryon budget), while $\sim 50\%$ of the baryons remains elusive to robust direct detection.

Looking for these "missing" baryons is crucial for the validity of our standard cosmology model. The standard theory of hierarchical structure formation models indicates that the majority of baryons exist between galaxies as the diffuse intergalactic medium (IGM). Numerical simulations in the standard cosmology further suggest that a large portion of this IGM is in the form of warm-hot intergalactic medium (WHIM) (Cen & Ostriker 1999; Davé et al. 2001; Cen & Ostriker 2006) with temperature $10^5\mathrm{K} < \mathrm{T} < 10^7$ K, which is believed to reside in moderately overdense structures such

⋆ Email:jwshao@shao.ac.cn
† Email:pjzhang@shao.ac.cn

as filaments. On one hand, this kind intergalactic medium is ionized dominantly by collisions, and is transparent to Lyα radiation, and thus is hard to trace by Lyα forest. The absorption signature toward a bright X-ray source is also too weak to be resolved by current spectrographs. On the other hand, though WHIM emits radiation in the UV and soft X-ray bands, the emission strength is too weak for current instruments to detect. There have been observations trying to detect WHIM via absorption and radiation signature, but many of them are of low significance or misinterpreted. See (Bregman 2007) for a recent review of the status of WHIM detections.

Among the methods of probing missing baryons, the Sunyaev Zel'dovich (SZ) effect is one of the most promising. Our universe is almost completely ionized after $z = 6$, where free electrons are prevailing in galaxy clusters as high energy ICM and in the less overdense filamentary structures as IGM. Free electrons will scatter off CMB photons through inverse Compton scattering, and generate secondary CMB temperature anisotropies, which is known as the Sunyaev Zel'dovich effect. Therefore, the SZ effect is contributed by virtually all electrons. In principle, from the SZ observations, we are able to find all electrons and hence all baryons, due to the electric neutrality of the universe.

The two major categories of the SZ effect are the thermal SZ effect (tSZ), arising through the thermal motion of electrons, and the kinetic SZ effect (kSZ), arising through the bulk motion of electrons. The efficiency for given electrons to generate the SZ effect is proportional to the thermal temperature for the thermal SZ effect and is proportional to the bulk peculiar velocity for the kinetic SZ effect. Since the thermal temperature of electrons strongly couples to the electron density, the dominant contribution to the thermal SZ effect comes from the high-density and high-temperature ICM. For example, White et al. (2002) found that 75% of the total thermal SZ effect at multipole $\ell < 2000$ comes from virialized regions with gas overdensity $\delta_{\rm gas} > 100$ and Hernández-Monteagudo et al. (2006) found similar results: 80% of the tSZ signal comes from collapsed structures. Since the missing baryons are likely in less dense regions with lower temperature, the ability to find missing baryons through the thermal SZ effect is limited.

On the other hand, the kinetic SZ effect has a better potential to probe the missing baryons. The peculiar velocity is determined by the large scale gravitational potential and is thus only weakly coupled to local mass concentration. Hence, the contribution to the kSZ effect is roughly proportional to the total mass of each baryon component, e.g., ICM and IGM. Namely, it is an approximately unbiased probe of baryons, regardless of their thermal state (as long as they are ionized). Since the mass fraction of the missing baryons is $\sim 50\%$, we thus expect a comparable contribution to the kSZ effect from the missing baryons. This makes the kinetic SZ effect a promising probe of the missing baryons. For example, there have been works studying the contribution of kSZ effect by WHIM to the CMB anisotropies (Atrio-Barandela et al. 2008; Génova-Santos et al. 2009).

The remaining question is to measure the kinetic SZ effect, for which there are several obstacles. First of all, the signal of the kinetic SZ effect is not only weak, but also lack of spectral features to extract from the overwhelming primary CMB. Thus, from the CMB measurement alone, we only expect to detect it in the auto power spectrum measurement at $\ell \gtrsim 3000$, where the primary CMB damps significantly and the kinetic SZ effect begins to dominate (e.g. Ma & Fry 2002; Zhang et al. 2004), and at $\nu = 217$ GHz frequency band, where the (non-relativistic) thermal SZ effect vanishes. However, refer to an interesting paper by Nozawa et al. 2006 concerning the residual tSZ effect at 217GHz due to the relativistic corrections by massive clusters. Other contaminations such as the dusty star-forming galaxies (Hall et al. 2010) make the kSZ detection even more difficult. For these reasons, even for CMB experiment as advanced as Planck, which has multiple bands over wide frequency range, it is difficult to detect the kinetic SZ effect directly, given its limited angular resolution. Secondly, like the thermal SZ effect, the kinetic SZ effect suffers from severe projection effect. It measures the electron momentum projected along the line of sight, thus the redshift information of baryons is entangled in the projection with a projection length of the size of the horizon. This not only degrades its power to infer the evolution of missing baryons over the cosmic epoch, but could also lead to large bias. For example, the patchy reionization could contribute a significant fraction to the kinetic SZ effect (Zahn et al. 2005; McQuinn et al. 2005; Iliev et al. 2007). Without redshift information, unless the reionization process is well understood and interpreted appropriately, the extra contribution from patchy reionization could be misinterpreted as the sign of missing baryons. It's interesting to notice the work of Hernández-Monteagudo & Ho (2009), which proposed to recover the signature of the bulk flow of the missing baryons by cross correlating future CMB data sets with kSZ estimates in galaxy clusters.

In this paper, we propose a kinetic SZ tomography method to overcome the above obstacles. The basic idea is to cross correlate the CMB observation with a galaxy redshift survey or other surveys of the large scale structure with sufficiently accurate redshift information such as the 21cm intensity mapping (Chang et al. 2008). Due to the cancellation mechanism arising from the underlying directional dependence of the kinetic SZ signal as a result of its vector nature, direct cross correlation between the kinetic SZ effect and the galaxy number density vanishes (refer to Fig. 1 for more detailed explanation). This differs significantly from the tight correlation between the thermal SZ effect and the galaxy density (Zhang & Pen 2001; Shao et al. 2009). One way to circumvent this cancellation is to square the kinetic SZ effect and measure its correlation with galaxies (Doré et al. 2004; DeDeo et al. 2005).

We propose an alternative approach to avoid the cancellation. One can reconstruct the peculiar velocity field from the galaxy spectroscopic redshift survey, weigh it with the observed galaxy number density and other redshift-dependent factors to reconstruct a weighted momentum field. This weighted *momentum* field has roughly the same directional dependence as the true kSZ signal and thus avoids the cancellation. We thus expect a measurable cross correlation between the reconstructed field and the CMB map, which extracts the kSZ component in the CMB temperature fluctuation.

The cross correlation signal should arise solely from the corresponding redshift range where galaxies reside, to an excellent approximation for a reasonably thick galaxy redshift bin ($\Delta z \gtrsim 0.2$) and sufficiently small angular scales ($\ell \gtrsim 10$). Thus it disentangles the kinetic SZ contribution in this redshift range from contributions of any other redshifts and recovers the redshift information of the kinetic SZ effect. It is for this reason that we dubbed this method as *the kinetic SZ tomography*, analogous to the thermal SZ tomography and also to the well known lensing tomography. An immediate application of the kinetic SZ tomography is to separate the patch reionization from the late time kinetic SZ effect. It is also effective to eliminate contaminations from the primary CMB, thermal SZ and other foreground contaminations, which do not have the characteristic directional dependence and thus should be uncorrelated with the reconstructed momentum field. Since the galaxy surveys usually have excellent signal to noise (S/N), the cross correlation measurement can achieve much higher S/N than the auto

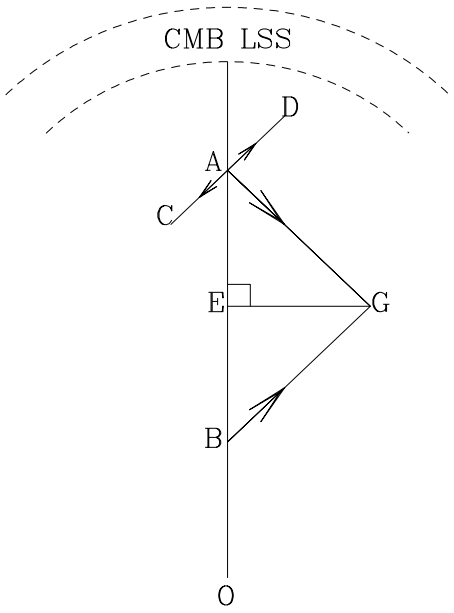

Figure 1. The vanishing correlation between the kinetic SZ effect and the galaxy number density. The line of sight is from the observer (O), through the points B, E and A, to the last scattering surface. One galaxy resides at point G and we shall discuss the velocity distribution given the existence of this galaxy. The line EG is perpendicular to the line of sight and AE=EB. The velocity at any point along the line of sight, e.g., the point A, can be decomposed, with respect to the position of the given galaxy, into one component along the direction AG and one perpendicular to the direction AG. The perpendicular component has equal probability to be along the direction AC or the direction AD and thus the net contribution to the kinetic SZ-galaxy cross correlation is zero. So the only velocity component which may contribute is the one along the direction AG. However, from the symmetry argument, if the evolution effect (light cone effect) can be neglected, velocity at point B has an equal probability to have a component along the direction BG, with the same amplitude. The projection of the two onto the line of sight cancels exactly. So the cross correlation between the kinetic SZ effect and the galaxy density vanishes.

correlation measurement of the kinetic SZ effect from the SZ surveys alone. Later we will show that, PLANCK plus BigBOSS can detect the kinetic SZ effect at $\sim 50\sigma$ level.

At the beginning stage of this work, Ho et al. (2009) published a work based on similar idea, whose applicability is further confirmed in this paper. The two works are carried out independently and thus differ in many details. We test the proposed kSZ tomography against a controlled set of hydrodynamical simulations and quantify the tightness of correlations between the reconstructed map and the true kSZ signal at various redshifts over $0 < z < 2$. We further investigate several complexities such as redshift distortion and feedback, and demonstrate the robustness of the kSZ tomography against various complexities. Both works confirm the power of the kSZ tomography.

The paper is organized as follows. In §2, we introduce the kSZ tomography method and discuss its limitations in general. We then test it against our hydrodynamic simulations in §3. The reconstruction and the test are done in both the real space (§3.1) and the redshift space (§3.2). In this section, we approximate galaxies as dark matter particles. So it corresponds to idealized surveys of virtually infinite galaxies such that shot noise in galaxy distribution is negligible. Realistic surveys have much lower galaxy number density and thus shot noise in the galaxy distribution induces non-negligible reconstruction noise. We directly quantify it from our simulations with a proper scaling (§4.1). We are then able to forecast its performance for survey combinations like the Planck CMB experiment plus the BigBOSS spectroscopic redshift survey (§4). We discuss and conclude in §5. We present more technical details and further discussions in the two appendices.

2 THE KINETIC SZ TOMOGRAPHY

Bulk motions of free electrons induce secondary CMB anisotropies, namely the kinetic Sunyaev Zel'dovich (kSZ) effect (Sunyaev & Zeldovich 1972, 1980), with temperature fluctuations

$$\begin{aligned}\Theta(\hat{n}) &\equiv \frac{\Delta T|_{\rm kSZ}}{T_{\rm CMB}} = \int \chi_e \bar{n}_e \sigma_T \frac{(1+\delta_e)\mathbf{v}\cdot\hat{n}}{c} \exp[-\tau(z)] a d\chi \\ &\equiv \int \mathbf{p}_\parallel W_{\rm kSZ}(z) d\chi \\ &\equiv \sum_i \Theta_i \; ; \; \Theta_i = \int_{\chi_i-\Delta\chi_i/2}^{\chi_i+\Delta\chi_i/2} \mathbf{p}_\parallel W_{\rm kSZ}(z) d\chi \; , \end{aligned} \quad (1)$$

where Θ_i is the contribution from electrons in the i-th redshift bin, spanning the comoving coordinate range $\chi_i - \Delta\chi_i/2 < \chi < \chi_i + \Delta\chi_i/2$. χ is the comoving radial coordinate, c is the speed of light and τ is the Thompson optical depth. $\mathbf{p} \equiv (1+\delta_e)\mathbf{v}$ is the (normalized) electron momentum and the subscript "$\parallel$" denotes the projection along the line of sight. δ_e is the electron number overdensity, and $\mathbf{v}$ is the electron peculiar velocity. The weighting function $W_{\rm kSZ} = \chi_e \bar{n}_e \sigma_T \exp(-\tau) a/c$ modulates the contribution from each redshift. Throughout the paper, we focus on the kSZ effect after reionization and thus set $\chi_e = 1$, an excellent approximation. Due to the neutrality, $\delta_e = \delta_{\rm gas}$, where $\delta_{\rm gas}$ is the overdensity of (ionized) gas.

As a vector, $\mathbf{p}$ can be always decomposed into a gradient (irrotational) part $\mathbf{p}_E$ and curl (rotational) part $\mathbf{p}_B$, $\mathbf{p} \equiv \mathbf{p}_E + \mathbf{p}_B$, where $\nabla \times \mathbf{p}_E = 0$ and $\nabla \cdot \mathbf{p}_B = 0$ respectively. Here, the "E" and "B" notations are analogous to the electromagnetic fields. As can be inferred from Eq. 1, the contribution from the gradient part is largely canceled out when integrating along the line of sight, as long as the weighting function $W_{\rm kSZ}$ varies slowly across a correlation length of $\mathbf{p}_E$, which is of the order 100 Mpc/h today.[1]. For the kinetic SZ effect after reionization, $W_{\rm kSZ}$ only changes significantly over the Hubble scale, thus the contribution from the gradient part is negligible and the only significant contribution comes from $\mathbf{p}_B$ (Vishniac 1987).

$\mathbf{p}_B$ in general has two sources of contribution. Since $\nabla \times \mathbf{p}_B = \nabla \times \mathbf{p} = (1+\delta_e)\nabla \times \mathbf{v} + \nabla\delta_e \times \mathbf{v}$, the B-mode of $\mathbf{p}$ can come from the B-mode of $\mathbf{v}$ or from the cross talk between the density and velocity. Following the same notation, we can decompose the velocity into a "E" mode (gradient part) $\mathbf{v}_E$ and a "B" mode (rotational part) $\mathbf{v}_B$. For purely gravitational interaction, the velocity "B" mode decays, until multi-streaming and shell crossing arise due to the nonlinear evolution (see for example chapter 2 of Bernardeau et al. 2002 for a discussion). Thus in the linear and weakly nonlinear regimes a good approximation is $\mathbf{v} = \mathbf{v}_E$ and the only contribution to the kSZ effect comes from the cross talk between the density

[1] This condition can be violated at the epoch of reionization, where the patchy reionization causes W to vary significantly over $\sim 10h$/Mpc scales.

gradient and the velocity. This is the well known Ostriker-Vishniac (OV) effect (Ostriker & Vishniac 1986; Vishniac 1987). In the nonlinear regime, $\mathbf{v}_B$ grows and can also contribute to the kSZ effect (Zhang et al. 2004).

The kinetic SZ tomography that we propose requires combination of a SZ survey and a galaxy spectroscopic redshift survey with overlapping sky coverage. It contains three major steps:

- Construct a 2D map $\hat{\Theta}_i$ from the 3D distribution of galaxies in the *i*-th redshift bin. Ideally, $\hat{\Theta}_i$ should be tightly correlated with Θ_i, the true kinetic SZ signal from this redshift bin. A crucial ingredient to guarantee a tight correlation is to estimate the peculiar velocity through the 3D galaxy distribution and use it to construct $\hat{\Theta}_i$. Hereafter, we often neglect the subscript "*i*" where it does not cause confusion.
- Cross correlate the reconstructed $\hat{\Theta}$ with a overlapping SZ survey. The cross correlation signal, to an excellent approximation, solely comes from the kinetic SZ in the chosen redshift bin. It is this step that recovers the redshift information of the kinetic SZ effect, eliminates various contaminations and reduces statistical errors.
- Interpret the *measured* cross correlation signal and reconstruct the true kinetic SZ signal. Trick similar to the one adopted in the thermal SZ tomography (Shao et al. 2009) can also be applied here.

The current paper will focus on the first two steps and only briefly discuss the third step.

2.1 The kinetic SZ reconstruction

The primary goal of this paper is to extract the kSZ signal as well as its redshift information through cross correlating SZ surveys with galaxy spectroscopic redshift surveys. As explained early, the usual two-point cross correlation between the kinetic SZ effect Θ and galaxy overdensity δ_g vanishes ($\langle\Theta\delta_g\rangle = 0$), due to the cancellation of positive and negative velocities along the line of sight (Fig. 1). A natural step to avoid such cancellation is to recover the velocity information and weigh the galaxies accordingly. This can be done in spectroscopic galaxy redshift surveys.

Spectroscopic galaxy redshift surveys, such as LAMOST[2], BOSS[3], BigBOSS[4], SKA[5], Euclid[6] and JDEM/ADEPT[7], will measure the 3D galaxy distribution $\delta_g(\mathbf{x})$. At least part of them will overlap with SZ surveys such as ACT[8], SPT[9] and PLANCK[10] on the sky coverage. We are able to recover the velocity field from $\delta_g(\mathbf{x})$ and then $\hat{\Theta}$, the galaxy momentum properly weighted. Since the direction of the peculiar velocity is taken into account in $\hat{\Theta}$, the cross correlation $\langle\hat{\Theta}\Theta\rangle$ no longer suffers from the usual cancellation and thus $\langle\hat{\Theta}\Theta\rangle \neq 0$.

In the linear regime, the mass conservation (i.e. *the continuity equation*) reduces to

$$\dot{\delta}_m + \nabla\cdot\mathbf{v} = 0\,, \tag{2}$$

where δ_m is the matter overdensity and $\mathbf{v}$ is the peculiar velocity of the matter field. In the same regime, namely at large scale, the 3D galaxy distribution is a good proxy of the underlying 3D matter distribution. This can be described by a galaxy bias $\delta_g = b_g\delta_m$. Under the above condition, given the observed 3D galaxy distribution $\delta_g^{\rm obs}(\mathbf{x})$, we are able to obtain an estimator of the velocity field, which in Fourier space reads

$$\hat{\mathbf{v}}(\mathbf{k}) = -if\,H\delta_g^{\rm obs}(\mathbf{k})\frac{\mathbf{k}}{k^2}\,, \tag{3}$$

where $\mathbf{k}$ is the 3D wave vector, $f \equiv d\ln D/d\ln a$ and D is the linear density growth rate. The superscript "hat" in $\mathbf{v}$ ($\hat{\mathbf{v}}$) and in other symbols (e.g. $\hat{\Theta}$) denotes the reconstructed quantity. In reality, to suppress the noise and stabilize the reconstruction, we often apply some filters to the density field, before applying Eq. 3. So $\delta_g^{\rm obs}$ should be treated as the smoothed density field.

Eq. 3 is a *biased* estimator of the true peculiar velocity $\mathbf{v}$. (1) The galaxy bias causes $\hat{\mathbf{v}}$ to be overestimated by a factor b_g. (2) Redshift distortion causes the observed density to deviate from the underlying matter density and thus biases the velocity reconstruction. (3) Nonlinearities in the density evolution causes deviation from Eq. 2. (4) In the nonlinear regime where shell crossing and multi-streaming happen, velocity vorticity (rotational part, or curl part) develops, which is completely missed by the estimator Eq. 3.

The imperfectness of the velocity reconstruction is not as severe as it looks, for the kinetic SZ tomography. Later we will show that the performance of the kSZ tomography is insensitive to deterministic errors in the velocity reconstruction. Thus a deterministic galaxy density and velocity bias, uncertainties in f and H, linear redshift distortion (the Kaiser effect) do not degrade the kSZ tomography. However, stochastic errors from stochastic galaxy bias, nonlinearities in the evolution of density and velocity do. Later we will quantify their impacts and show them to be moderate at relevant scales.

With the 3D density field δ_g and thereby the recovered 3D velocity field $\hat{\mathbf{v}}$ in hand, we can then reconstruct a weighted 2D momentum map

$$\hat{\Theta} \equiv \int d\chi\hat{\mathbf{p}}_\parallel\hat{W}(z)\,, \tag{4}$$

where $\hat{\mathbf{p}} \equiv (1+\delta_g^{\rm obs})\hat{\mathbf{v}}(\mathbf{x})$, and $\hat{\mathbf{v}}(\mathbf{x})$ is the inverse Fourier transform of $\hat{\mathbf{v}}(\mathbf{k})$. We choose the weighting function $\hat{W}(z) = W_{\rm kSZ}(z)$. The integral in Eq. 4 is over the corresponding redshift bin. Again, we can also apply some filters to the density field, before taking the product in $\hat{\mathbf{p}}$. These filters are not necessary to be the same as the ones for the velocity reconstruction. Furthermore, the density measurement in the product may not even be the same as the one used in the velocity measurement, as correctly pointed by Ho et al. (2009).

Here we want to clarify a likely confusing point. As discussed before, the kinetic SZ effect is mainly contributed by $\mathbf{p}_B$ instead of $\mathbf{p}_E$. On the other hand, the reconstructed $\hat{\mathbf{v}}$ in Eq. 3 is actually $\mathbf{p}_E$, which becomes clear later in Eq. 8. It thus seems that the reconstruction misses the dominant contribution to the kinetic SZ effect and thus should fail to work. However, there is an extra factor $(1+\delta_g)$ in the estimator $\hat{\Theta}$ (Eq. 4). Recall that, in the OV effect (Ostriker & Vishniac 1986; Vishniac 1987), it is the cross-talk between the density gradient and the curl-free velocity that generates a curl component in $\mathbf{p}$. Here, the cross-talk between the density and $\mathbf{p}_E$ generates a B-mode in the reconstructed $\hat{\mathbf{p}}$, which is tightly correlated with the true $\mathbf{p}_B$ on relevant scales. This explains the reasonable performance of the reconstruction technique and the kinetic SZ tomography.

[2] http://www.lamost.org/website/en
[3] http://cosmology.lbl.gov/BOSS/
[4] http://bigboss.lbl.gov/index.html
[5] http://www.skatelescope.org/
[6] http://sci.esa.int/euclid
[7] http://jdem.gsfc.nasa.gov/
[8] http://www.physics.princeton.edu/act/index.html
[9] http://pole.uchicago.edu/
[10] http://www.rssd.esa.int/index.php?project=planck

2.2 How to quantify the kSZ tomography performance?

The estimator $\hat{\Theta}$ is certainly imperfect. It can have both systematical and random offsets with respect to Θ. These deviations should be both scale and redshift dependent. These deviations can be visualized by a Θ-$\hat{\Theta}$ plot. Alternatively, it can be quantified by two parameters, r and $b_{\hat{\Theta}}$. r describes the tightness of the $\hat{\Theta}$-Θ correlation[11] and $b_{\hat{\Theta}}$ is the bias in $\hat{\Theta}$ with respect to Θ. Clearly, both r and $b_{\hat{\Theta}}$ depend on the redshift range of galaxies used for reconstruction. We want to quantify the redshift dependence of r and b. Thus later in the analysis we will choose a projection length across which evolutions in r and b_Θ are negligible. For such projection, r and $b_{\hat{\Theta}}$ are functions of z and the 2D wave vector $k_\perp$, the inverse of the perpendicular spatial separation,

$$r(k_\perp, z) \equiv \frac{P_{\hat{\Theta}\Theta}(k_\perp, z)}{\sqrt{P_{\hat{\Theta}}(k_\perp, z) P_\Theta(k_\perp, z)}} , \tag{5}$$

and

$$b_{\hat{\Theta}}(k_\perp, z) \equiv \sqrt{\frac{P_{\hat{\Theta}}(k_\perp, z)}{P_\Theta(k_\perp, z)}} , \tag{6}$$

Later we will recognize $\mathbf{k}_\perp$ as the perpendicular component of the usual 3D wave vector $\mathbf{k}$. The Ps are the corresponding power spectra.

There is no guarantee that $b_{\hat{\Theta}}$ is close to unity, even in the linear regime. As explained earlier, the velocity estimation is biased. Further, in the product $\hat{\Theta} \propto (1 + \delta_g^{\rm obs})\hat{\mathbf{v}}$, $\delta_g^{\rm obs}$ is also biased with respect to δ_e. Later in the Appendix A we will show the complicated behavior of $b_{\hat{\Theta}}$.

However, large deviation of $b_{\hat{\Theta}}$ from unity does not necessarily mean poor performance of the kinetic SZ tomography, for three reasons. (1) First, the signal-to-noise ratio (S/N) of the $\langle \Theta\hat{\Theta} \rangle$ measurement, is solely determined by r. The S/N of each mode (Fourier or multipole mode) is

$$\begin{aligned} \left(\frac{S}{N}\right)^2 &= \frac{P_{\Theta\hat{\Theta}}^2}{P_{\Theta\hat{\Theta}}^2 + (P_\Theta + P_\Theta^N)(P_{\hat{\Theta}} + P_{\hat{\Theta}}^N)} \\ &= \frac{1}{1 + r^{-2}\left(1 + \frac{P_\Theta^N}{P_\Theta}\right)\left(1 + \frac{P_{\hat{\Theta}}^N}{P_{\hat{\Theta}}}\right)} , \end{aligned} \tag{7}$$

where P_Θ^N and $P_{\hat{\Theta}}^N$ are the corresponding noise power spectra. We find that the $b_{\hat{\Theta}}$ dependence drops out in the error estimation. A rescaling $\hat{\Theta} \to b_{\hat{\Theta}}\hat{\Theta}$ leaves no effect on the S/N of the cross correlation measurement, since both $P_{\hat{\Theta}}^N, P_{\hat{\Theta}} \propto b_{\hat{\Theta}}^2$ and r is unchanged under this scaling. (2) $b_\Theta \neq 1$ definitely affects the expectation value of the cross correlation. However, since in the theoretical interpretation of the measured cross correlation, one can take the galaxy bias, redshift distortion and possibly other complexities into account and thus avoid systematical errors induced by $b_\Theta \neq 1$ reasonably well. (3) Based on the same technique in the thermal SZ tomography (Shao et al. 2009), we can combine the cross correlation measurement $P_{\Theta\hat{\Theta}}$ and the auto correlation measurement $P_{\hat{\Theta}}$ to obtain $P_\Theta = P_{\Theta\hat{\Theta}}^2/(r^2 P_{\hat{\Theta}})$. This estimation relies on no information of $b_{\hat{\Theta}}$ and thus avoids the bias problem.

[11] r that we define differs from the one defined in Ho et al. (2009). First, their r is for the velocity field instead of the momentum field, 3D instead of 2D. Second, their r is not the cross correlation coefficient, but is actually analogous to r/b of the 3D velocity field, in our notation.

For these reasons, in the main text we will focus on r to quantify the performance of the kinetic SZ tomography and leave discussion on $b_{\hat{\Theta}}$ in the Appendix A.

2.3 Origins of the stochasticity $r \neq 1$

A number of approximations made in the reconstruction pipeline cause the stochasticity in the Θ-$\hat{\Theta}$ relation ($r \neq 1$). (1) First of all, as an approximation to the exact mass conservation equation

$$\dot{\delta}_m + \nabla \cdot (1 + \delta_m)\mathbf{v} = 0 , \tag{8}$$

the starting point Eq. 2 only holds where $\delta_m \ll 1$. (2) From Eq. 2 to Eq. 3, we have made assumptions of linear evolution ($\delta_m(k, z) \propto D(z)\delta_m(k, z_i)$), deterministic bias between δ_g and δ_m, and curl-free velocity. None of these approximations are exact in the nonlinear regime. (3) Even under these assumptions, Eq. 2 and 3 only hold in real space. Namely, we have implicitly assumed that the observed $\delta_g^{\rm obs}$ is the galaxy overdensity δ_g in real space ($\delta_g^{\rm obs} = \delta_g$). However, in reality, what we directly measure is the galaxy number overdensity δ_g^s in redshift space ($\delta_g^{\rm obs} = \delta_g^s$). Due to the redshift distortion, $\delta_g^s \neq \delta_g$. The δ_g^s-δ_g relation is stochastic, due to nonlinear mapping between redshift and real space, nonlinearities in both the density and velocity fields (e.g. White et al. 2009) and velocity vorticity (Carlson et al. 2009). (4) Even if we have perfect E-mode velocity reconstruction, we still have no handle on the B-mode velocity, which contributes the kinetic SZ effect. (5) In Eq. 4, we multiply the reconstructed velocity with $1 + \delta_g^{\rm obs}$ instead of $1 + \delta_e$. The possible stochasticity between δ_e and δ_g also increases the stochasticity between Θ and $\hat{\Theta}$.

With the aid of our hydrodynamic simulation, we are able to quantify the combined influence of all these factors on r, except for the stochastic galaxy bias. Ho et al. (2009) used the halo occupation model and N-body simulations to produce galaxy mock catalog. This approach captures the galaxy stochasticity and shows that the kSZ tomography is robust against it. Our simulations have relatively small box size ($100h^{-1}$Mpc) and hence do not allow us to follow the same approach. So we leave this issue for further investigation.

3 TESTING AGAINST HYDRODYNAMICAL SIMULATIONS

We test the kinetic SZ tomography against our hydrodynamical simulations. The simulations are run with the GADGET2 code (Springel 2005) in a ΛCDM cosmology with parameters: $\Lambda = 0.732$, $\Omega_0 = 0.268$, $\Omega_b = 0.044$ $h = 0.71$, $\sigma_8 = 0.85$. The box size of the simulation is $L = 100h^{-1}$ Mpc on each side, in which 512^3 dark matter particles and 512^3 gas particles are initially seeded (See more details about the simulation in Jing et al. 2006; Lin et al. 2006). We have an non-adiabatic run, in which gas particles are allowed to cool and condense into collisionless star particles, along with which SN feedback is taken into account. We also have an adiabatic run with the same cosmological parameters and the same initial conditions. We will focus on the non-adiabatic run, since it has better capture on the gastrophysics and hence better modeling of the kinetic SZ effect. Unless otherwise specified, all simulations are based on this simulation. We also analyze the adiabatic run to better understanding the generality of the kSZ tomography (§3.3.2). We choose in this work a few representative redshifts to quantify the feasibility of the tomography technique, which is mainly characterized by the quantity $r(k_\perp, z)$.

Our hydrodynamic simulations have direct information of the gas momentum distribution and thus the kinetic SZ effect. However, the simulations don't simulate galaxies. To proceed, we approximate galaxies as simulation dark matter particles. Since the galaxy stochasticity is likely sub-dominant (Bonoli & Pen 2009; Baldauf et al. 2010) , this approximation is reasonable to estimate r between $\hat{\Theta}$ and Θ, although it indeed over-estimates it. As demonstrated by Ho et al. (2009), the kSZ tomography is robust against the galaxy stochasticity. So we will leave this issue elsewhere. Since the number density of simulation particles is much higher than that of galaxies in any realistic surveys, shot noise in the $\hat{\Theta}$ reconstruction is negligible. To use the measured r for forecasting, we have to take the shot noise inevitable in realistic surveys into account. We leave this issue until next section.

We test the kinetic SZ tomography at several typical redshifts $z = 0, 0.53, 1.02, 2.08$. We reconstruct the velocity and consequently the momentum field from the dark matter distribution in the corresponding simulation outputs. At these redshifts, we project the 3D momentum field over a single box size ($100h^{-1}$ Mpc) to get the 2D momentum maps. We then compare these maps with the maps of underlying kinetic SZ signal, which is directly measured by multiplying the gas density and velocity distribution in the corresponding simulation outputs. Since the simulations have information of peculiar velocity, we carry out the reconstruction and comparison in both real space and redshift space.

3.1 The reconstruction in real space

3.1.1 The reconstruction procedure

We first carry out the reconstruction in real space. The reconstruction is a two-step process. The first step is to reconstruct the peculiar velocity. At each redshift z_i, we construct the matter density field $\delta(\mathbf{x})$ using clouds-in-cells (CIC) scheme in a partitioning of $n_g^3 = 256^3$ cells, followed by a Fourier transform to get the matter distribution in Fourier space $\delta(\mathbf{k})$. We then apply a Gaussian filter[12] $W_G(k) = \exp(-k^2R_s^2/2)$ to the original field $\delta(\mathbf{k})$ in order to wipe off nonlinear fluctuations on small scales, which are uncorrelated with the large scale velocity. The adopted smoothing length $R_s = 1.56h^{-1}$ Mpc applied in the whole context is around the radius of a typical cluster, and we will discuss the influence of different smoothing length in §3.3.1. We then obtain the reconstructed velocity $\hat{\mathbf{v}}(\mathbf{k})$ from Eq. 3 through this smoothed density field. By the inverse Fourier transform, we obtain the real space velocity field $\hat{\mathbf{v}}(\mathbf{x})$.

The second step is to project the momentum field along the line of sight $\hat{n}$ to get the reconstructed 2D map at redshift z_i

$$\hat{\Theta}_{j1,j2}(\hat{\mathbf{n}}) = \sum_{j3} \hat{\mathbf{n}} \cdot \frac{\hat{\mathbf{v}}_{j1,j2,j3}}{c}(1+\delta_{j1,j2,j3}) \,. \tag{9}$$

Since the weighting function $W_{\rm kSZ}$ changes little over that scales, so we treat it as a constant and omit it. The sum is over a single simulated box at the investigated redshift, instead of stacking the box in the light cone. Notice that the density term in the above equation (Eq. 9) is the unsmoothed density, which preserves the necessary information of the true density field in the deriving of the momentum field. In practice, we construct at each redshift three maps along three Cartesian coordinate directions of the simulated box respectively. As they can be considered as three independent measurements, in the following figures which concern statistics, we show the average results unless specified.

[12] Ho et al. (2009) populated halos with galaxies. Since in that case the galaxy density is low, and shot noise is non-negligible, they applied the Wiener filter to reduce the Poisson noise. This is also a necessary procedure when dealing with real data. In our work, we use simulation particles as galaxies, whose number density is much higher and thus the shot noise is negligible. For this reason, we instead apply generally a Gaussian window function to filter out small scale nonlinear fluctuations.

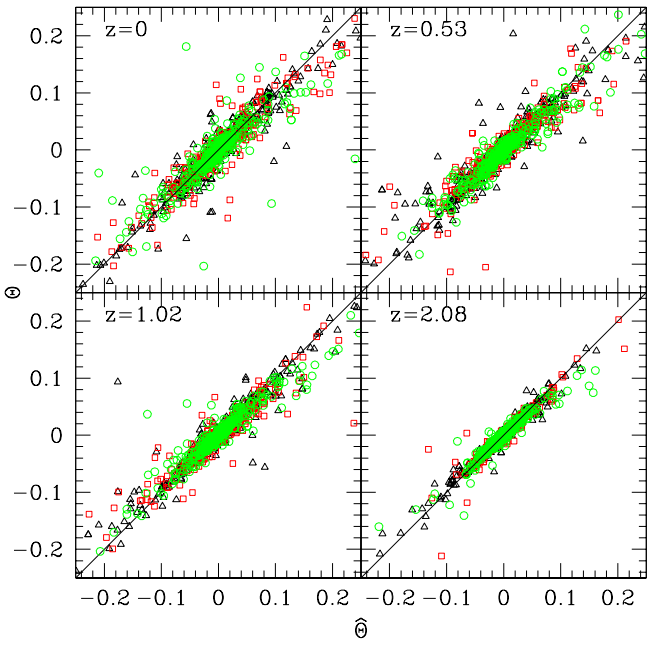

Figure 2. The $\hat{\Theta}$-Θ map (in arbitrary unit) in the real space at z=0, 0.53, 1.02, 2.08. In order to further reduce the scattering of $\hat{\Theta}$-Θ relation, we average the recovered velocity field in every neighboring $4^3 = 64$ cells to get the averaged velocity field $\hat{\mathbf{v}}$ as well as the density field δ on a much coarser partitioning, say, 64^3 cells. We show here the cell-to-cell correspondence in all three Cartesian directions by randomly selecting 512 out of 64^3 couples. The recovered $\hat{\Theta}$ field intimately follows the kSZ signal along the diagonal at high redshifts, while at low redshift, there are great fluctuations due to non-linear evolution of the density field and thereby the velocity field. The three components in Cartesian directions are denoted by different point types, triangles for x, squares for y and circles for z.

At the same time, we obtain the *true* kSZ signal in a similar way

$$\Theta_{j1,j2}(\hat{\mathbf{n}}) = \sum_{j3} \hat{\mathbf{n}} \cdot \frac{\mathbf{v}_{b,j1,j2,j3}}{c}(1+\delta_{b,j1,j2,j3}) \,, \tag{10}$$

where δ_b is the nonlinear overdensity of baryons. $\mathbf{v}_b$ is the bulk velocity derived directly from the simulation by averaging within the host cell (j1,j2,j3)

$$\mathbf{v}_b = \frac{\sum_i \mathbf{v}_i m_i w_i}{\sum_i m_i w_i} \,, \tag{11}$$

where $\mathbf{v}_i$ and m_i are the comoving peculiar velocity and the mass of i-th gas particle in the host cell. w_i is a spline kernel used to smooth the gas particles.

3.1.2 The $\hat{\Theta}$-Θ relation

In Figure 2 we show the cell-to-cell $\hat{\Theta}$-Θ correspondence. The $\hat{\Theta}$-Θ data points scatter around $\hat{\Theta} = \Theta$, meaning a bias $b_\Theta \sim 1$. However,

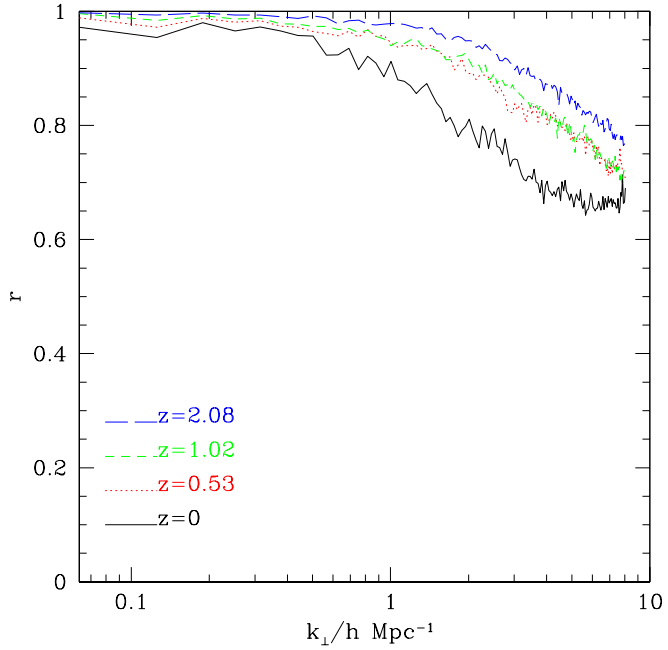

Figure 3. The cross correlation coefficients r between $\hat{\Theta}$ and Θ. The correlation coefficient is averaged over the three components. The two are highly correlated, r≃0.9, on large scale $k_\perp \leqslant 1h\,\mathrm{Mpc}^{-1}$ for all the 4 redshifts, while less correlated to smaller scales ends due to the non-linearities coming into play. Nevertheless, the correlation coefficient is still tight at z=0, with $r > 0.6$ up to $k_\perp \sim 8h\,\mathrm{Mpc}^{-1}$.

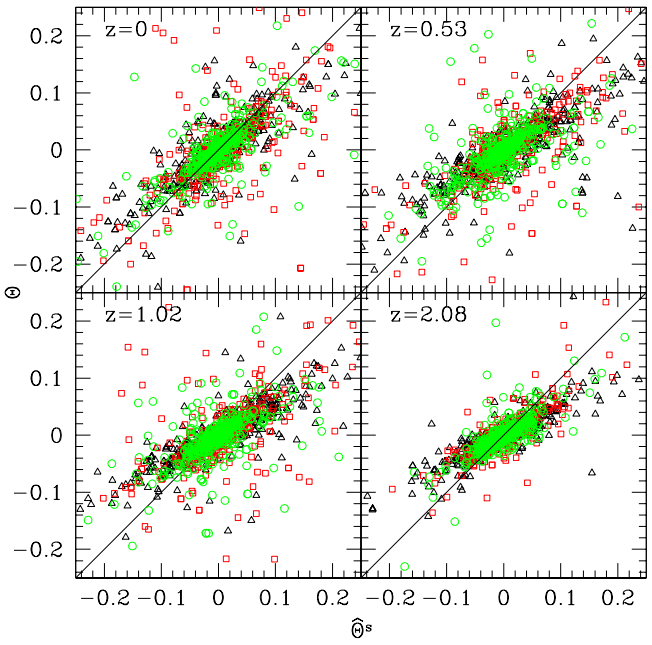

Figure 4. The Θ-$\hat{\Theta}^s$ relation in the redshift space. The same routine as Fig. 2 is used in deriving this relation. At high redshifts, the recovered $\hat{\Theta}^s$ overweighs the underlying kSZ signal Θ, because the Kaiser effect enhances the density by a factor $\sim 1 + f/3$, and the higher redshift the higher the slope is, since $f \simeq \Omega_m^{0.6}(z)$ is larger at early epochs. On the other hand, the scatters in Θ-$\hat{\Theta}^s$ is much larger than that in the real space due to the larger stochasticities of density-velocity relation and the real space-redshift space mapping.

this should not be over-emphasized since this only represents an unrealistic case of galaxy bias $b_g = 1$ without redshift distortion. Reconstructions based on galaxy sample with $b_g \neq 1$ would result in $b_\Theta \neq 1$ and hence a different slope of the $\hat{\Theta}$-Θ relation. Redshift distortion also changes the slope of the $\hat{\Theta}^s$-Θ relation, as can be seen from Fig. 4.

The $\hat{\Theta}$-Θ relation shows non-negligible dispersion around the mean, but still reasonably tight. This means that the stochasticity is noticeable, but not yet overwhelming. We also notice that, the dispersion gets stronger at lower redshift. This is not surprising, since the reconstruction is based on linear theory and thus works better at higher redshift. Nonlinearities in the density field and velocity field degrades the reconstruction accuracy, as discussed in §2.3.

3.1.3 The cross correlation coefficient r

Out of the two quantities concerning to the reconstruction performance, the cross correlation coefficient r describes the tightness of $\hat{\Theta}$-Θ relation and is a major measure of the kinetic SZ tomography. $b_{\hat{\Theta}}$ is of less importance in quantifying the kSZ tomography performance, so we leave related results to the Appendix A. To measure them, we perform 2D Fourier transforms of Θ ($\hat{\Theta}$). $\Theta(\mathbf{k}_\perp) = \int d^2\mathbf{x}_\perp \Theta(\mathbf{x}_\perp) \exp(i\mathbf{k}_\perp \cdot \mathbf{x}_\perp)/A$, where A is the area of the map. Note here $\mathbf{k}_\perp$ and $\mathbf{x}_\perp$ are both 2D variables. We then obtain the power spectrum P_Θ with $(2\pi)^2\delta_D(\mathbf{k}_\perp - \mathbf{k}_\perp{}')P_\Theta(k_\perp) = \langle\Theta(\mathbf{k}_\perp)\Theta(\mathbf{k}_\perp{}')\rangle$.

Fig. 3 shows that the stochasticity in the $\hat{\Theta}$-Θ relation is in general not a severe issue, even in the strongly nonlinear regime, consistent with Fig. 2. As shown we have strong correlations, $r \gtrsim 0.9$ to $k_\perp = 1h\,\mathrm{Mpc}^{-1}$at all redshifts, and even $r \gtrsim 0.8$ to $k_\perp \sim 3h\,\mathrm{Mpc}^{-1}$except z=0. Nonlinearities do degrade the reconstruction, as we see that r decreases towards low redshifts. However, even at $z = 0$, the $\hat{\Theta}$-Θ correlation is still pretty tight, with $r > 0.6$ to $k_\perp \sim 8h\,\mathrm{Mpc}^{-1}$. We don't correct for the aliasing effect, such that small scale results may be misleading (Jing 2005). Nevertheless, we do expect good results up to a quarter of the Nyquist wavenumber, i.e. around $2h\,\mathrm{Mpc}^{-1}$, and it's safe for us to estimate the cross power spectrum up to $\ell \sim 2000 - 3000$.

3.2 The reconstruction in redshift space

In reality, what we get from a galaxy survey is the galaxy number density in the redshift space. As expected in §2, the redshift space distortion will induce new sources of uncertainty and further degrades the reconstruction. We are able to quantify its impact through our simulations. Due to its own peculiar motion, the apparent position of each dark matter particle along the line of sight can be written as

$$x^s = x + \frac{\mathbf{v}\cdot\hat{\mathbf{n}}}{H}\,, \tag{12}$$

where $\hat{\mathbf{n}}$ denotes the unit vector along the line of sight, and $\mathbf{v}$ is the comoving peculiar velocity. $\mathbf{x}^s$ is position in the redshift space, and from here on the superscript "^{s}" indicates the corresponding quantity in the redshift space. As a result of this displacement, what we observed is a distorted density field δ^s. With δ^s as the starting point, we can reconstruct the momentum fields $\hat{\Theta}^s$ through Eq. 3, following the same procedure as in the real space.

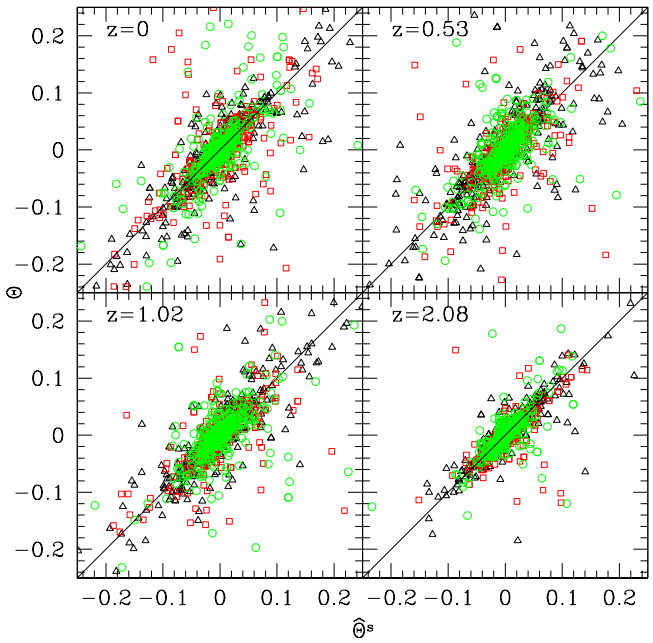

Figure 5. The Θ-$\hat{\Theta}^s$ relation in the redshift space after correcting for the Kaiser effect. It's interesting to find that the slopes approach unity at all investigated redshifts, while the scatters keep nearly unchanged compared to Fig. 4.

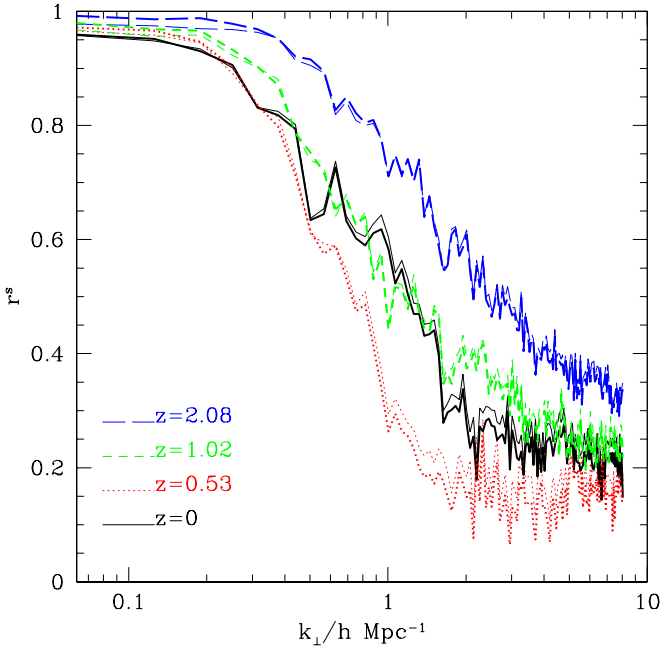

Figure 6. The cross correlation coefficients $r(k_\perp, z)^s$ in the redshift space. Thick lines show r^s with Kaiser effect corrected for. Compared to Fig. 3, $r(k_\perp, z)^s$ is suppressed throughout all scales, especially at $k_\perp \gtrsim 1h\,\mathrm{Mpc}^{-1}$. At $z \lesssim 1$, the reconstruction works poorly, with $r \simeq 0.3$ on scales $k_\perp \gtrsim 3h\,\mathrm{Mpc}^{-1}$. However, there's a considerable correlation strength $r^s \gtrsim 0.5$ for $k_\perp \lesssim 1h\,\mathrm{Mpc}^{-1}$at z=0. At higher redshift where nonlinearity of velocity is not significant, the correlation strength is still tight enough, e.g. with $r \simeq 0.7$ for $k_\perp \sim 1h\,\mathrm{Mpc}^{-1}$at z=2.08.

3.2.1 Θ-$\hat{\Theta}^s$ *relation in the redshift space*

The Θ-$\hat{\Theta}^s$ relation is shown in Fig. 4, which is significantly different from the one in real space (Fig. 2). We can see that in two aspects. (1) The average slope of the Θ-$\hat{\Theta}$ relation changes, from $\hat{\Theta} \simeq \Theta$ to $\hat{\Theta} \simeq a\Theta$ with $a > 1$. This is caused by the linear redshift distortion (the Kaiser effect), which induces

$$\delta^s(\mathbf{k}) = \delta(\mathbf{k})(1 + \beta\mu_k^2), \tag{13}$$

where $\mu_k = \hat{\mathbf{n}} \cdot \hat{\mathbf{k}}$ is the cosine of the angle between the line of sight $\hat{\mathbf{n}}$ and the wavevector $\mathbf{k}$. $\beta = f/b_g$. The Kaiser effect enhances the galaxy overdensity by a factor $\simeq 1 + \beta/3 > 1$ and thus causes the slope $a > 1$. We also notices that the slope a decrease from high redshifts to low redshifts. There are two causes. First, $\beta = f \simeq \Omega_m^{0.6}(a)$ (Peebles 1980) (in our case where $b_g = 1$) decreases with decreasing redshift. Second, the finger of God effect caused by small scale random motion suppresses the redshift space galaxy density. This effect becomes stronger at lower redshift. (2) Scatters in the Θ-$\hat{\Theta}^s$ relation are significantly larger than that in the real space (Fig. 2). Stochasticities in the density-velocity relation and real space-redshift space mapping are largely responsible for these larger scatters.

It's interesting to show the Θ-$\hat{\Theta}^s$ relation if we correct for the Kaiser effect. The figure is shown in Fig. 5. We find that the slopes approach unity at all investigated redshifts, while the scatters keep nearly unchanged compared to Fig. 4. This is, however, not unexpected, since the deterministic Kaiser formula only changes the amplitude and is reversible given cosmology. Thus finger of God should be mainly responsible for the scatters of the relation.

3.2.2 $r^s(k_\perp, z)$ *in the redshift space*

The cross correlation coefficient r in redshift space is shown in Fig. 6. Compared to Fig. 3, the correlation coefficient is suppressed throughout all scales, especially at $k_\perp \gtrsim 1h\,\mathrm{Mpc}^{-1}$. At $k_\perp \gtrsim 3h\,\mathrm{Mpc}^{-1}$and $z \lesssim 1$, the kinetic SZ reconstruction and thus the kinetic SZ tomography works poorly since the reconstructed $\hat{\Theta}$ barely resembles the true signal Θ ($r \lesssim 0.3$). These results show unambiguously that redshift distortion is a significant source of error in the kinetic SZ tomography. It's also worthwhile to see the changes if we correct for the Kaiser effect. They're also shown in Fig. 6 as thick lines. As indicated by Fig. 5, correcting for the Kaiser effect does not influence r^s too much on scales of interest.

As explained in §2.3, the degradation is caused by the stochasticity in the δ-δ^s relation. They can be induced by the nonlinear mapping between the real space density and the redshift space density (e.g. Scoccimarro 2004) and the stochasticity between the density and velocity field (e.g. White et al. 2009). This stochasticity then induces the stochasticity in the reconstructed velocity $\hat{\mathbf{v}}$, with respect to true velocity (Eq. 3). In the momentum reconstruction we need to multiply the reconstructed velocity by an extra factor $1 + \delta$ (Eq. 4) to obtain the reconstructed momentum. So the stochasticity in the momentum reconstruction and thus the kinetic SZ reconstruction has an extra source, from the term $1 + \delta$. All these complexities worsen the reconstruction, increase scatters in Θ-$\hat{\Theta}$ and decrease r.

Despite the above degradations, the reconstructed $\hat{\Theta}$ still shows reasonably tight correlation with the true signal Θ at $k_\perp \lesssim 1h\,\mathrm{Mpc}^{-1}$. We will show in the next section that this correlation

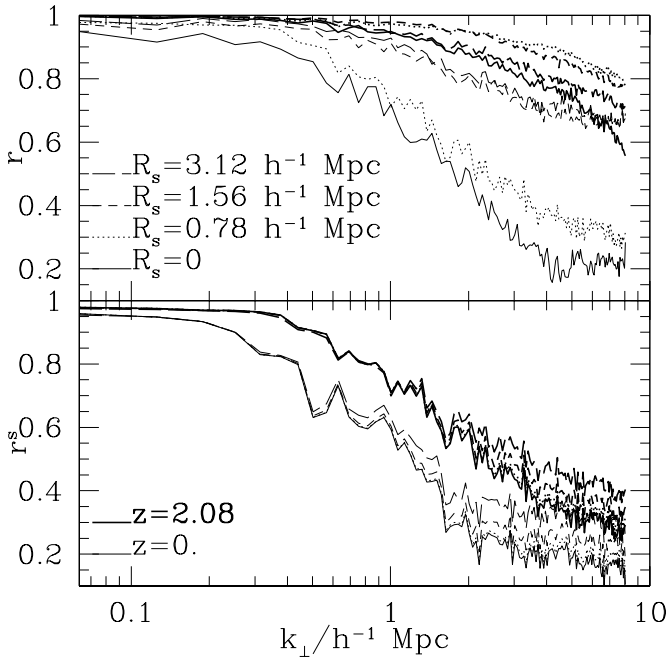

Figure 7. The deviations between different smoothing scales, say, 0, $0.78h^{-1}$ Mpc , $1.56h^{-1}$ Mpc and $3.12h^{-1}$ Mpc , in both real space (top panel) and redshift space (bottom panel). In the real space, smoothing length with $0.78h^{-1}$ Mpc works best at z=2.08 while $3.12h^{-1}$ Mpc is the most suitable at z=0. However, in the redshift space, the enhancement due to smoothing is less effective, and a larger smoothing length is better. Probably an anisotropic smoothing other than a Gaussian smoothing should work better. As a median smoothing length, $1.56h^{-1}$ Mpc is effective at both low and high redshift.

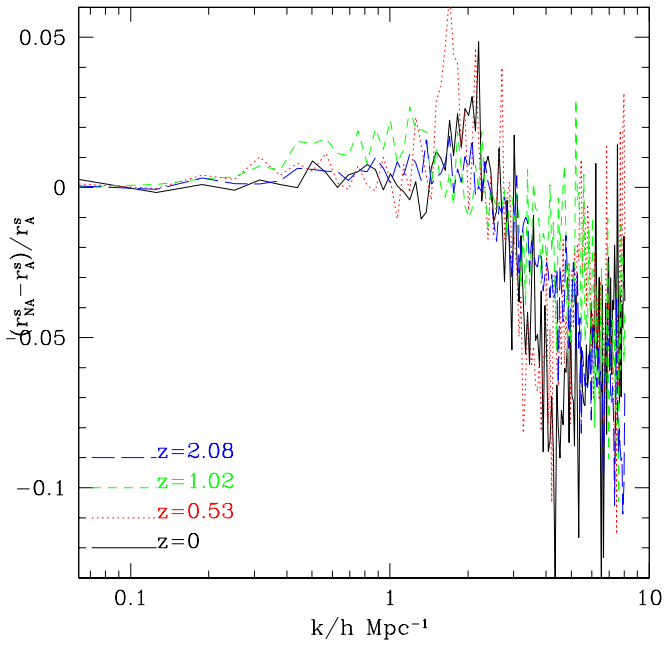

Figure 8. The difference of the correlation coefficient between adiabatic and non-adiabatic simulations. The overall r^s is insensitive to gastrophysics, and there're only ~2-3% changes of r^s. It will accordingly influence the estimator of the signal-to-noise of the cross power spectrum by several percent level, however, for kSZ tomography, this is sufficient for the current surveys.

strength allows for robust kinetic SZ tomography, combining the Planck CMB experiment and the BigBOSS galaxy spectroscopic redshift survey, or other surveys with comparable power.

An interesting behavior to notice is that r^s at $z = 0.53$ is worse than at $z = 0$. This result is consistent with a larger scatters in the Θ-$\hat{\Theta}$ plot at $z = 0.53$ than at $z = 0$, implying that stochasticities induced by the Finger of God effect becomes the largest at that epoch. At redshift higher than $z \sim 1$, the reconstruction suffers less from the nonlinearities and is thus stronger, e.g. with $r > 0.7$ at $k_\perp < 1h$/Mpc at z=2.08. Actually, we find in simulations that the comoving velocity dispersion peaks at $z \sim 0.6$. This would induce the largest anisotropies and hence make r^s at $z \sim 0.6$ the worst.

3.3 Uncertainties in r

In the above section, we quantify the impact of redshift distortion on r and thus show that redshift distortion degrades the kinetic SZ reconstruction significantly. There are other factors affecting the reconstruction. Here, we briefly discuss the influence of filters adopted to smooth the density field (§3.3.1) and gastrophysics (§3.3.2).

3.3.1 The influence of density smoothing on r

The results shown above all adopt a Gaussian filter with smoothing length $R_s = 1.56h^{-1}$ Mpc to smooth the density field before velocity reconstruction. The reconstruction robustness no wonder depends on the way to smooth the density field. We do not aim to perform a comprehensive investigation on this issue. Rather, we will restrict to the Gaussian filter and investigate the dependence of r on R_s. We arbitrarily compare between the cases of $R_s = 0, 0.78, 1.56, 3.12$ h^{-1} Mpc . For clarity, we only show the comparisons at $z = 0$ and $z = 2.08$ in Fig. 7 .

The basic (and obvious) conclusion is that, smoothing is necessary to suppress small scale nonlinearities and improve the reconstruction. Fig. 7 (upper panel) shows general improvement in r when smoothing is taken, comparing to the case of no smoothing ($R_s = 0$). For example, smoothing the density field with $R_s = 1.56h^{-1}$ Mpc can boost r by $\sim$ 30% at $k = 1h\,\mathrm{Mpc}^{-1}$and a factor of 2 or more at smaller scales, in real space.

Gaussian smoothing is less effective in redshift space: the improvement in r_s is often less than 10% on scales of interest (bottom panel, Fig. 7). The redshift space overdensity is anisotropic, so a spherical Gaussian smoothing will not work well. An anisotropic filter may work better in redshift space. This is certainly an interesting technical issue for further investigation.

A right smoothing should balance between suppressing small scale nonlinearities and preserving large scale signal. If R_s is too large, it may wipe off too much large scale clustering responsible for peculiar velocity and thus degrade the reconstruction (decrease r). This may be the reason that $R_s = 0.78h^{-1}$ Mpc works better than larger R_s, at $z = 2.08$ in the real space. However, overall $R_s = 1.56$ h^{-1} Mpc works reasonably well at all redshifts investigated.

The simulation data we deal with is like an ideal survey, with negligible shot noise, uniform selection function and regular survey boundary. Smoothing for real data is of course much more complicated. For example, a big issue in real survey is shot noise due to low galaxy number density, especially in spectroscopic redshift sur-

veys. For this issue, one can refer to Ho et al. (2009) for discussion on the application of the Wiener filter.

3.3.2 r and gastrophysics

r also depends on gastrophysics. All the results shown above are based on our non-adiabatic simulation, with radiative cooling, star formation and supernova feedback. Although we are not able to robustly quantify its detailed dependence on these gastrophysical processes, we can obtain a rough estimation by comparing the above results to our adiabatic simulation with identical initial conditions. The relative differences of r^s between the two simulations are shown in Fig. 8. We find that, overall r and thus the performance of the kinetic SZ tomography is insensitive to the gastrophysics. r at $k_\perp < 1h\,\mathrm{Mpc}^{-1}$only varies by less than 2-3%. The influence of gastrophysics is larger at smaller scales, but is still less than 5% up to $k_\perp = 3h\,\mathrm{Mpc}^{-1}$.

This insensitivity to gastrophysics has two implications on our kinetic SZ tomography. First, it is unlikely that some realistic gastrophysical process not included in our non-adiabatic simulation can dramatically suppress r and thus invalidates the tomography. Second, this significantly simplifies the theoretical interpretation of the tomography results. Based on the same technique in (Shao et al. 2009) , we can combine the two *measured* correlations, $\langle\Theta\hat{\Theta}\rangle$ and $\langle\hat{\Theta}\hat{\Theta}\rangle$, to obtain $\langle\Theta\Theta\rangle$ arising from the same redshift bin. The only unknown quantity in this approach is r, which we shall calibrate against simulations. However, if r is very sensitive to gastrophysics, the calibration on r would be very difficult due to large uncertainties in our theoretical and numerical understanding of these gastrophysics. The insensitivity of r to gastrophysics shown in Fig. 8 implies that, despite imperfect theoretical and numerical understanding of these gastrophysics, r can still be accurate to a few percent level at relevant scales. This precision suffices for the kinetic SZ tomography.

4 ERROR FORECAST

The r measured above quantifies the performance of the kinetic SZ tomography for a virtually ideal galaxy survey, for which the simulation particle number density is high and the shot noise is negligible. However, in real surveys, the galaxy number density is a factor of 10^4-10^5 smaller, resulting in much larger and thus non-negligible shot noise. The shot noise affects both the velocity and momentum reconstruction. We use our simulation to quantify these effects and then apply these results to forecast the performance of the kinetic SZ tomography. Our target CMB experiment is Planck and the target galaxy spectroscopic survey is BigBOSS (Schlegel et al. 2009). The kinetic SZ tomography based on other SZ surveys like SPT and galaxy surveys like ADEPT, Euclid and SKA is expected to work better.

4.1 Estimating the reconstruction noise from galaxy distribution shot noise

The discreteness of dark matter particles induces spurious fluctuations (shot noise) in the density field, which we denote as δ_N, and thereby in the reconstructed velocity, which we denote as $\mathbf{v}_N$. The correlation of the contaminated momentum $\hat{\Theta}_c$ is (for simplicity, we omit the projection along the line of sight)

$$\begin{aligned}\langle\hat{\Theta}^s_c(\hat{n})W\hat{\Theta}^s_c(\hat{n}')\rangle \;\propto\; & \langle(1+\delta^s+\delta_N)(\hat{\mathbf{v}}^s+\hat{\mathbf{v}}_N)\cdot\hat{n}\\ & \times(1+\delta^{s\prime}+\delta'_N)(\hat{\mathbf{v}}^{s\prime}+\mathbf{v}'_N)\cdot\hat{n}'\rangle\\ = \;& \langle(1+\delta^s)\hat{\mathbf{v}}^s\cdot\hat{n}(1+\delta^{s\prime})\hat{\mathbf{v}}^{s\prime}\cdot\hat{n}'\rangle\\ & +\langle(1+\delta^s)\mathbf{v}_N\cdot\hat{n}(1+\delta^{s\prime})\mathbf{v}'_N\cdot\hat{n}'\rangle\\ & +\langle\delta_N\hat{\mathbf{v}}^s\cdot\hat{n}\delta'_N\hat{\mathbf{v}}^{s\prime}\cdot\hat{n}'\rangle\,.\end{aligned}$$

The last two terms in the above equation are the leading non-vanishing noise terms. We denote the first noise term as $N_1 \propto (1+\delta^s)\mathbf{v_N}$ while the second as $N_2 \propto \delta_N\hat{\mathbf{v}}^s$

By randomizing the particle positions in the simulation, we can directly measure δ_N and derive therein $\mathbf{v}_N \propto \delta_N(k)\hat{k}/k$. Following the same procedure as in reconstructing the momentum map, we produce two corresponding maps of these two shot noises. In order to estimate the contribution of shot noise, we compute the power spectrum of the two noise terms, and show the ratios $P_{N_{1,2}}/P_{\hat{\Theta}^s}$ in Fig. 9. We can see that both the P_{N_1} and P_{N_2} noise terms are much smaller than the reconstructed momentum powers. Although N_1 and N_2 terms are comparable on the very large scales, they deviate significantly towards smaller scales, with N_2 terms predominantly overweighing N_1 terms. On the small scales, N_2 terms would turn out to be several thousandth of the reconstructed momentum $\hat{\Theta}^s$, and they can be comparable to or even dominate the signal, given a much smaller number density in current galaxy redshift surveys. Nevertheless, on scales of interest for kSZ tomography, say $k_\perp \lesssim 1h\,\mathrm{Mpc}^{-1}$, galaxy surveys would provide a relatively less contaminated reconstruction of the momentum.

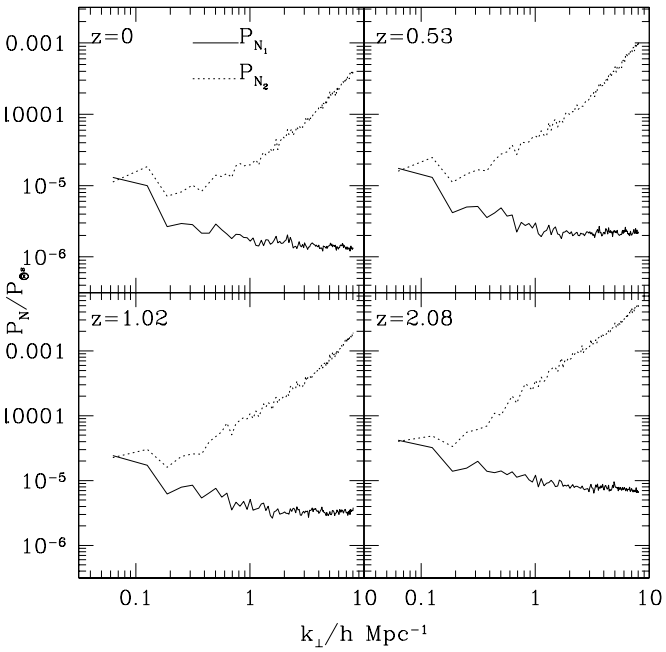

Figure 9. The ratio $P_{N_{1,2}}/P_{\hat{\Theta}^s}$ of the shot noise power spectrum and the reconstructed momentum power spectrum. Both the $\Delta^2_{N_1}$ and $\Delta^2_{N_2}$ are much smaller than the reconstructed momentum powers, with N_2 terms dominating N_1 towards smaller scales. Given a small number density in current galaxy redshift survey, the total shot noise would be comparable to the signal. Nevertheless, on scales of interest for kSZ tomography, say $k_\perp \lesssim 1h\,\mathrm{Mpc}^{-1}$, galaxy surveys would provide a relatively less contaminated reconstruction of the momentum.

4.2 Error forecast in C_l

Based on the above results, we are able to estimate the S/N for real surveys. Since in this section we consider the error forecast in real survey, i.e. in the redshift space, we omit the superscript "^{s}" for simplicity. For a given redshift bin $\in [z-\Delta z/2, z+\Delta z/2]$, we are able to measure the angular cross power spectrum C_ℓ between the reconstructed $\hat{\Theta}$ and the CMB measurement where the kSZ effect is embedded. The statistical error in this measurement can be estimated by

$$\frac{\Delta C_\ell}{C_\ell} \simeq \sqrt{\frac{1+\frac{C_\ell^{\rm CMB}+C_\ell^{\rm kSZ}+C_\ell^{\rm CMB,N}}{r^2 C_\ell^{\rm kSZ,\Delta z}}(1+\frac{C_{\hat{\Theta}}^N}{C_{\hat{\Theta}}})}{2\ell\Delta\ell f_{\rm sky}}} \simeq \frac{1}{2r\ell\Delta\ell f_{\rm sky}}\sqrt{\frac{C_\ell^{\rm CMB}+C_\ell^{\rm kSZ}+C_\ell^{\rm CMB,N}}{C_\ell^{\rm kSZ,\Delta z}}\left(1+\frac{C_{\hat{\Theta}}^N}{C_{\hat{\Theta}}}\right)}. \quad (14)$$

Here, $C_\ell^{\rm CMB}$ is the angular power spectrum of primary CMB and $C_\ell^{\rm CMB,N}$ is the power spectrum of the measurement noise. The thermal SZ effect is also a source of noise. Since we work with the frequency band around 217 Ghz, where the thermal SZ effect virtually vanishes, we will neglect the thermal SZ effect. There are other possible sources of error, such as the dusty star forming galaxies and radio sources. They are not likely dominant over the primary CMB at $\ell \lesssim 2000$ of our interest. Thus we will not include them in the error analysis. $C_\ell^{\rm kSZ}$ is the angular power spectrum of the kinetic SZ effect and $C_\ell^{\rm kSZ,\Delta z}$ is the contribution from the given redshift bin. $C_{\hat{\Theta}}^N/C_{\hat{\Theta}}$ is the ratio of the angular power spectrum of the reconstruction shot noise and of the reconstructed momentum $\hat{\Theta}$. r is again the cross correlation coefficient between the reconstructed kSZ map and the true kSZ signal. However, now the projection length is in general much larger than the simulation box size $100h^{-1}$Mpc. For interesting angular scales of $\ell \sim 10^3$, two redshift bins separated by more than $100h^{-1}$Mpc can be approximated as uncorrelated. So we can average over r measured in the last section over the relevant redshift range to obtain an estimation of the r used in this section.

The first factor 1 in the r.h.s of Eq. 14 comes from the cosmic variance in the cross-correlation signal and assumes the kinetic SZ effect and the reconstructed $\hat{\Theta}$ are Gaussian. The actual non-Gaussianties will increase the cosmic variance. However, this cosmic variance term is sub-dominant to the other term, since $(C_\ell^{\rm CMB}+C_\ell^{\rm kSZ}+C_\ell^{\rm CMB,N})/C_\ell^{\rm kSZ,\Delta z} \gg 1$ and $r \leqslant 1$. So the Gaussian assumption is reasonable. And the second relation holds since usually $(C_\ell^{\rm CMB}+C_\ell^{\rm kSZ}+C_\ell^{\rm CMB,N})/C_\ell^{\rm kSZ,\Delta z} \gg 1$.

From this equation, we can figure out the improvement in S/N of the kinetic SZ measurement. To better see this point, we will discuss under the limit that the galaxy number density is sufficiently high such that $C_{\hat{\Theta}}^N/C_{\hat{\Theta}} \ll 1$ at sufficiently large angular scales. We then have

$$\frac{S}{N} \sim \sqrt{\frac{r\times 2\ell\Delta\ell f_{\rm sky} C_\ell^{\rm kSZ,\Delta z}}{C_\ell^{\rm CMB}+C_\ell^{\rm kSZ}+C_\ell^{\rm CMB,N}}}. \quad (15)$$

We can compare it to the S/N of the kSZ auto correlation power spectrum measurement

$$\frac{S}{N} \sim \sqrt{\ell\Delta\ell f_{\rm sky}}\frac{C_\ell^{\rm kSZ}}{C_\ell^{\rm CMB}+C_\ell^{\rm kSZ}+C_\ell^{\rm CMB,N}} \quad (16)$$

As $C_\ell^{\rm CMB} \gg C_\ell^{\rm kSZ}$ at $\ell \lesssim 2000$, the improvement in S/N by the kSZ tomography is of the order $r\sqrt{C_\ell^{\rm CMB}/C_\ell^{\rm kSZ}}\sqrt{C_\ell^{\rm kSZ,\Delta z}/C_\ell^{\rm kSZ}}$. Since r is close to unity at relevant scale (e.g. $\ell \sim 10^3$ and $z \sim 1$), for a sufficiently deep galaxy survey (e.g. to $z = 2$ or beyond), the overall improvement is of the order $\sqrt{C_\ell^{\rm CMB}/C_\ell^{\rm kSZ}} \gg 1$. In reality, since the galaxy number density is finite, shot noise dominates at small scales, as can be inferred from Fig. 9.

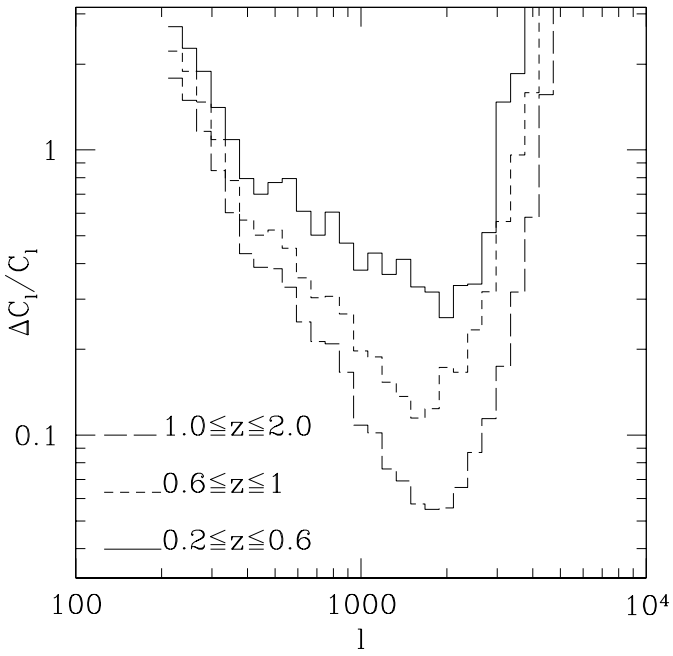

Figure 10. The error of the measurements of cross power spectrum between at redshift bins z=0.2 − 0.6, 0.6 − 1.0 and 1.0 − 2.0, using BigBOSS plus PLANCK. There are significant signals around $\ell \sim 2000$, with errors 26%, 11% and 6% respectively for the three redshift bins. With a larger redshift bin and better r^s over the relevant multipole ranges, the total S/N in z = 1.0 − 2.0 is 46, the more considerable than the other two, 10 at z=0.2-0.6 and 21 at z=0.6-1.0.

Now we numerically calculate the S/N for the combination of PLANCK plus BigBOSS-N. $C_\ell^{\rm CMB}$ is calculated from CAMB[13]. The instrument noise power spectrum of PLANCK is

$$C_\ell^{\rm CMB,N} = (\sigma_{p,T}\theta_{\rm FWHM})^2 W_\ell^{-2}, \quad (17)$$

where the window function $W_\ell = \exp(-\ell(\ell+1)/2\ell_{\rm beam}^2)$ for a Gaussian beam with $\ell_{\rm beam} = \sqrt{8\ln 2}/\theta_{\rm FWHM}$.[14] For PLANCK, $\theta_{\rm FWHM} = 5.0$ arcminutes. Within which the average 1σ sensitivity per pixel $\sigma_{p,T}/T_{\rm CMB} = 4.8\times10^{-6}$ is expected after 2 full sky surveys. PLANCK will survey the sky at several frequency bands. The 217 GHz band where thermal SZ signal vanishes is the one that we use to cross correlate with galaxies.[15] $C_\ell^{\rm kSZ}$ and $C_\ell^{\rm kSZ,\Delta z}$ are calculated by the model of Zhang et al. (2004).

For the target galaxy spectroscopic redshift survey, we choose the BigBOSS(-N) project (Schlegel et al. 2009). It plans to measure the spectroscopic redshifts of 30 million LRGs and emission line galaxies at $0.2 \leqslant z \leqslant 2$ over 14000 deg^2 sky coverage. Since

[13] http://camb.info/

[14] http://www.rssd.esa.int/index.php?project=planck

[15] The 217 GHz band is the only band promising to detect the kinetic SZ effect in auto correlations. However, the kSZ tomography is able to detect the kSZ effect in other frequency bands and the resulting S/N can be comparable at= $\ell < 2000$ where the thermal SZ effect is sub-dominant to the primary CMB. This is an issue for further investigation.

PLANCK will survey the full sky, the overlapping fractional sky coverage is $f_{\rm sky} = 14000/(4\pi/(\pi/180)^2)$. Given the much lower galaxy number density (comparing to simulations), shot noise is a significant source of error in the kinetic SZ tomography. The resulting reconstruction noise can be roughly estimated through a simple scaling

$$\frac{C^N_{\hat\Theta}(\ell)}{C_{\hat\Theta}(\ell)} \sim \frac{P_{N_1}(k_\perp)+P_{N_2}(k_\perp)}{P_{\hat\Theta}(k_\perp)}\frac{\Sigma_{\rm sim}}{\Sigma_{\rm obs}}\,, \qquad (18)$$

where, Ps are the ones at some intermediate redshift of the redshift bin and $k_\perp = \ell/\chi$. $\Sigma_{\rm sim}$ and $\Sigma_{\rm obs}$ are the surface densities in the simulation and in the real survey respectively. This estimation is by no means exact. But it is reasonably good to demonstrate the power of PLANCK plus BigBOSS to detect kSZ.

We divide the BigBOSS survey into three redshift bins, $0.2 \leqslant z \leqslant 0.6$, $0.6 \leqslant z \leqslant 1.0$ and $1.0 \leqslant z \leqslant 2.0$. This choice is somewhat arbitrary. In the error estimation, we simply adopt r and $C^N_{\hat\Theta}/C_{\hat\Theta}$ estimated at some intermediate redshift of each redshift bin. In the error estimation using Eq. 14, the multipoles ℓ are logarithmically equal spaced, say, $\Delta\ell/\ell = 12.2\%$. We present the error distribution of the cross power spectrum in Fig. 10. We find that the cross correlation can be measured robustly at $\ell \sim$ 1000-3000. For example, the relative errors at $\ell = 2000$ are about 26%, 11% and 6% at the three redshift bins correspondingly. Good performance at these scales is expected for three reasons. (1) $\hat\Theta$ and the underlying Θ are tightly correlated at corresponding scale $k_\perp = \ell/\chi$. (2) Shot noise is low for a galaxy survey as big as BigBOSS, comparing to the noise level in the kSZ measurement. (3) The primary CMB drops while the measurement shot noise is still bearable at $\ell = 2000$.

The accuracy of the cross power spectrum measurement increases with redshift. This is partly due to stronger r at higher redshift. And this epoch, the comoving scale $k_\perp = \ell/\chi(z)$ moves to more linear regime and the nonlinearity becomes weaker. Both push r upward and improve the kSZ tomography. What's more, the binned kSZ signal from z=1.0-2.0 is larger than the other two on scales of interest. It certainly helps the cross correlation measurement.

On the other hand, it is unlikely to detecting kSZ at $\ell \lesssim 300$ and $\ell \gtrsim 3000$ through the kSZ tomography with PLANCK plus BigBOSS-N . Toward larger scales, the kSZ signal decrease, while the primary CMB overweighs by 3 or 4 orders. On smaller scales, the finite angular resolution of the PLANCK survey causes the CMB measurement noise to increase exponentially. At the same time, the shot noise in BigBOSS begins to dominate over the galaxy clustering signal. Here we want to caution the readers that the S/N at $\ell \gtrsim 3000$ is overestimated, since we neglected noises from the dusty star forming galaxies (Hall et al. 2010), which may dominate over the primary CMB.

We estimate that, the overall S/Ns for the $z = 0.2-0.6$, 0.6-1.0 and 1.0-2.0 redshift bins are 10, 21 and 46, respectively. The combined S/N of the whole redshift range $z = 0.2-2.0$ is 51. These results are consistent with the findings of Ho et al. (2009), in which they use PLANCK plus SDSS and ADEPT. Although these numbers are likely only accurate within a factor of 2, they nevertheless robustly confirm the applicability of the proposed kSZ tomography to realistic surveys. Since the overall S/N$\sim$ 50, we are able to choose finer redshift bins and thus measure the kSZ evolution over $\sim$ 10 redshift bins.

5 DISCUSSIONS AND CONCLUSIONS

In this paper, we proposed the kSZ tomography method, tested it against simulations and estimated its applicability to realistic surveys. This methods requires a galaxy spectroscopic redshift survey to reconstruct the large scale peculiar velocity and then weigh the galaxy density with this velocity to produce a weighted galaxy momentum map $\hat\Theta$. By construction, this map is tightly correlated with the true kSZ signal and thus allows us to extract the kSZ signal from the CMB maps through the cross correlation measurement. Our work confirms the major finding of Ho et al. (2009), namely cross correlating the properly weighted galaxy momentum field with CMB fluctuations can significantly improve the kinetic SZ measurement. We estimate that BigBOSS-N plus PLANCK is able to measure the kSZ effect at 50σ confidence level, qualitatively consistent with results of Ho et al. (2009). Given this S/N, our method is able to recover the redshift distribution of the kSZ effect over $\sim$ 10 redshift bins.

Thanks to the hydrodynamical simulations at hand, we are able to better model the true kSZ signal and thus reduce one source of error in the analysis. We are also able to quantify the impact of redshift distortion, by performing the reconstruction in both real and redshift space. We find that redshift distortion is a major factor affecting the kSZ tomography. It degrades the performance, especially at small scales. However, we show that, its impact at $k_\perp \lesssim 1h$/Mpc is moderate and thus the kSZ tomography can still work reasonably well to scales $\ell \simeq k_\perp\chi \sim 3000$.

Comparing between the simulations with star formation, gas cooling and supernovae feedback turned on or off, we are able to quantify the impact of gastrophysics.We showed that the correlation coefficient r between the reconstructed $\hat\Theta$ and the true kSZ signal Θ is insensitive to gastrophysics of star formation, feedback and gas cooling included in our hydrodynamic simulations. This behavior is of crucial importance for the theoretical interpretation of the kSZ tomography result. It enables an approach similar to the thermal SZ tomography (Shao et al. 2009) to circumvent the problem of the potentially (and likely inevitably) large bias in $\hat\Theta$ with respect to Θ. This is an issue for further investigation.

The proposed kSZ tomography has unique advantages over detecting the kinetic SZ effect through auto-correlations. (1) By construction, the cross correlation measurement only picks up the kSZ component in CMB. Due to the lack of characteristic directional dependence, primary CMB, the thermal SZ effect, dusty star forming galaxies and any noise sources of scalar nature do not bias the cross correlation measurement. It is thus a rather clean way to eliminate the otherwise overwhelming systematical errors in the kSZ measurement. (2) It recovers the redshift information of the kSZ effect. The redshift information is not only useful to better understand the evolution of missing baryons, but also useful to separate the kSZ effect after reionization from the one due to patchy reionization. It thus allows for better understanding of the reionization process. (3) The relatively higher S/N of galaxy surveys help to beat down the statistical errors in the kSZ measurement, as we have shown for the combination of PLANCK plus BigBOSS-N.

We have carried out a concept study and shown the applicability of the kSZ tomography to real surveys. However, the analysis is simplified, with many issues left for future study. An incomplete list is as follows.

(i) The galaxy stochasticity. It definitely degrades the kSZ tomography performance. However, studies shown that the stochasticity in the galaxy bias is likely at the level of 10% or smaller (Bonoli & Pen 2009; Baldauf et al. 2010). So it is unlikely to com-

pletely invalidate the kSZ tomography, consistent with Ho et al. (2009) in which the stochasticity exists in their galaxy mock catalogue. Nonetheless, it is important to quantify the impact of galaxy stochastic bias.

(ii) The smoothing scheme. The actual galaxy density distribution is irregular, due to the intrinsic nonlinearities, galaxy shot noise and survey irregularities. So an important step is to smooth the density field and stabilize the velocity reconstruction. We have done simple study on the smoothing scheme in §3.3.1 and found that this is indeed important. For example, we find that a spherical Gaussian smoothing does not work in redshift space as well as in real space. Ho et al. (2009) investigated the Weiner filter to deal with galaxy shot noise. A comprehensive study is required to develop an optimal smoothing scheme.

(iii) The cosmic variance. Our simulated box size is not large enough to quantify the cosmic variance, as the correlation length of velocity is $\sim 100\ h^{-1}$ Mpc . Simulations with larger box size are required to study this issue, along with the galaxy stochasticity and smoothing scheme.

(iv) The robustness of modeling r, the cross coefficient r between the reconstructed $\hat{\Theta}$ and the true kSZ signal Θ. It plays a central role in quantifying the performance of the kSZ tomography and in converting the measured cross correlation signal to the kSZ auto correlation power spectrum. We have measured the impact of gastrophysics on r and found that, gastrophysics of star formation, supernovae feedback and gas cooling would only change r by several percent on scales of interest. We shall check this result against more comprehensive investigations on gastrophysics. We have measured the dependence of r on the smoothing length and found a strong dependence. This implies that r in real surveys which have complicated masks and noise distribution could differ from what we have presented here.

(v) Improvements on the forecast. The forecast can be improved by including other sources of contamination such as dusty star forming galaxies. It can also be extended to other combinations such as CMB experiments like ACT and SPT and many other galaxy spectroscopic redshift surveys. Dusty star forming galaxies do not have significant effect on the kSZ tomography based on PLANCK plus BigBOSS, since the applicable scale is $\ell \lesssim 3000$. At smaller scales approachable to ACT and SPT, dusty star forming galaxies overwhelm both the primary CMB and the thermal and kinetic SZ effect. So for these surveys, this source of error must be taken into account appropriately.

(vi) Probing missing baryons with the kSZ tomography. Although it is one of major motivations and the most important applications of the kSZ tomography, we have not carried out any quantitative analysis on this aspect. Our hydro simulations have rich information on the IGM. However, the simulation box is not sufficiently large to robustly quantify the contribution of the missing baryons to relevant statistics in the kSZ tomography. Furthermore, more comprehensive and robust treatments on gasdynamics and galaxy formation are demanded to reveal the connections between the kSZ effect and density and velocity of galaxies. Again, this requires more hydrodynamical simulations, which will be investigated elsewhere.

6 ACKNOWLEDGEMENT

We thank S. Ho for his insightful questions and suggestions to improve the paper. This work is supported in part by the National Science Foundation of China (grant No. 10533030, 10673022, 10821302, 10873027&10878001), the Knowledge Innovation Program of CAS (grant No. KJCX2-YW-T05 & KJCX3-SYW-N2), the 973 program grant No. 2007CB815401 & 2007CB815402 and the CAS/SAFEA International Partnership Program for Creative Research Teams. The simulations were done at Shanghai Supercomputer Center by the supports of Chinese National 863 project (grant No.06AA01A125).

REFERENCES

Atrio-Barandela, F., Mücket, J. P., Génova-Santos, R. 2008, ApJ, 674, L61
Baldauf, T., Smith, R. E., Seljak, U., Mandelbaum, R. 2010, PRD, 81, 063531
Bernardeau, F., Colombi, S., Gaztañaga, E., Scoccimarro, R. 2002, Physics Reports, 367, 1
Bonoli, S., Pen, U. L. 2009, MNRAS, 396, 1610
Bregman, J. N. 2007, Annual Review of Astronomy & Astrophysics, 45, 221
Carlson, J., White, M., Padmanabhan, N. 2009, PRD, 80, 043531
Cen, R., Ostriker, J. P. 1999, ApJ, 514, 1
Cen, R., Ostriker, J. P. 2006, ApJ, 650, 560
Chang, T.-C., Pen, U.-L., Peterson, J. B., McDonald, P. 2008, Physical Review Letters, 100, 091303
Davé, R., et al. 2001, ApJ, 552, 473
DeDeo, S., Spergel, D. N., Trac, H. 2005, arXiv:astro-ph/0511060
Doré, O., Hennawi, J. F., Spergel, D. N. 2004, ApJ, 606, 46
Fukugita, M., Peebles, P. J. E. 2004, ApJ, 616, 643
Fukugita, M., Peebles, P. J. E. 2006, ApJ, 639, 590
Génova-Santos, R., Atrio-Barandela, F., Mücket, J. P., Klar, J. S. 2009, ApJ, 700, 447
Hall, N. R., et al. 2010, ApJ, 718, 632
Hernández-Monteagudo, C., Trac, H., Verde, L., Jimenez, R. 2006, ApJ, 652, L1
Hernández-Monteagudo, C., Ho, S. 2009, MNRAS, 398, 790
Ho, S., Dedeo, S., Spergel, D. 2009, arXiv:0903.2845
Iliev, I. T., Pen, U.-L., Bond, J. R., Mellema, G., Shapiro, P. R. 2007, ApJ, 660, 933
Jing, Y. P. 2005, ApJ, 620, 559
Jing, Y. P., Zhang, P., Lin, W. P., Gao, L., Springel, V. 2006, ApJ, 640, L119
Kaiser, N. 1987, MNRAS, 227, 1
Lin, W.P., Jing,Y.P., Mao,S., Gao,L., McCarthy,I.G., 2006, ApJ, 651, 636
Ma, C.-P., Fry, J. N. 2002, Physical Review Letters, 88, 211301
McQuinn, M., Furlanetto, S. R., Hernquist, L., Zahn, O., Zaldarriaga, M. 2005, ApJ, 630, 643
Nozawa, S., Itoh, N., Suda, Y., & Ohhata, Y. 2006, Nuovo Cimento B Serie, 121, 487
Ostriker, J. P., Vishniac, E. T. 1986, ApJ, 306, L51
Peebles, P. J. E. 1980, *The Large Scale Structure of the Universe*, Princeton University Press, 1980.
Pueblas, S., Scoccimarro, R. 2009, PRD, 80, 043504
Schlegel, D. J., et al. 2009, arXiv:0904.0468
Scoccimarro, R. 2004, PRD, 70, 083007
Shao, J., Zhang, P., Lin, W., Jing, Y. 2009, arXiv:0903.5317
Springel, V., 2005, MNRAS, 364,1105
Sunyaev, R. A., Zeldovich, Y. B. 1972, Comments on Astrophysics and Space Physics, 4, 173
Sunyaev, R. A., Zeldovich, I. B. 1980, MNRAS, 190, 413
Vishniac, E. T. 1987, ApJ, 322, 597
White, M., Hernquist, L., Springel, V. 2002, ApJ, 579, 16

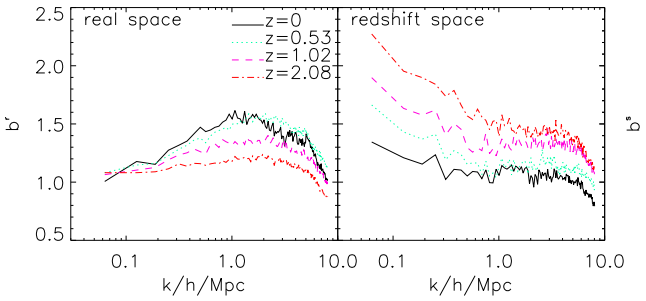

Figure A1. The reconstruction bias $b^r_{\hat\Theta}$ in the real space (left panel) and $b^s_{\hat\Theta}$ in the redshift space (right panel). In the real space, the reconstructed signal agree well with Θ at high redshifts on large scales up to $k_\perp \leqslant 1h\,\mathrm{Mpc}^{-1}$, while overestimates Θ by almost 60% at recent epochs. However, in the redshift space, the resulting $\hat\Theta^s$ powers are boosted on the largest scales due to the Kaiser effect, while on smaller scales, FOG effect dominates and brings down the powers, the severest at z=0.

White, M., Song, Y.-S., Percival, W. J. 2009, MNRAS, 397, 1348
Zahn, O., Zaldarriaga, M., Hernquist, L., McQuinn, M. 2005, ApJ, 630, 657
Zhang, P., Pen, U.-L. 2001, ApJ, 549, 18
Zhang, P., Pen, U.-L., Trac, H. 2004, MNRAS, 347, 1224

APPENDIX A: THE RECONSTRUCTION BIAS $B_{\hat\Theta}$

As we aim to reconstruct the kSZ map from the galaxy spectroscopic survey, it's important to assess the reconstruction process. Quantitatively, we use r (Eq. 5) and $b_{\hat\Theta}$ (Eq. 6) to figure out how well the reconstruction is. As explained in §2.2 of the main context, the S/N of the cross power spectrum (Eq. 7), which is what we are most concerned about the future observations, is solely dependent on the determination of the cross correlation coefficient r, while a biased $b_{\hat\Theta}$, i.e. the relative amplitude, does not influence the estimation of the signal to noise of the cross power spectrum. However, $b_{\hat\Theta}$ is a direct measure of the reconstruction bias, and it does reflect how the reconstructed field suffers from nonlinearity and the redshift space distortion. So we here address the behavior of $b_{\hat\Theta}$ both in the real space and the redshift space.

The results of $b^r_{\hat\Theta}$ and $b^s_{\hat\Theta}$ are shown respectively in the left and right panel of Fig. A1. We caution the readers to pay attention only to the relative differences between real and redshift space, or between different redshifts. The absolute value of b_Θ could be misleading, due to the simplistic assumption of $b_g = 1$.

In real space, $\hat\Theta$ tends to more over-estimate Θ at lower redshifts (b_Θ increases with redshift). In redshift space, it is the opposite case. This is likely caused by the competition between the linear redshift distortion (the Kaiser effect) and the Finger of God effect. The Kaiser effect (Kaiser 1987) enhances the clustering of matter along the line of sight and thus the derived velocity and Θ^s. This is the reason the redshift space b_Θ at $z = 2.08$ is larger than the real space b_Θ at the same epoch. On the other hand, the Finger of God effect (see Scoccimarro 2004 for reviews of the redshift space distortion and the FOG effect) suppresses the redshift space matter overdensity and hence Θ^s. The Finger of God effect is amplified by the nonlinearities with respect to the Kaiser effect, resulting in decreasing b_Θ with redshift. It is also responsible for the smaller b_Θ in redshift space at $z = 0$ comparing to the one in real space.

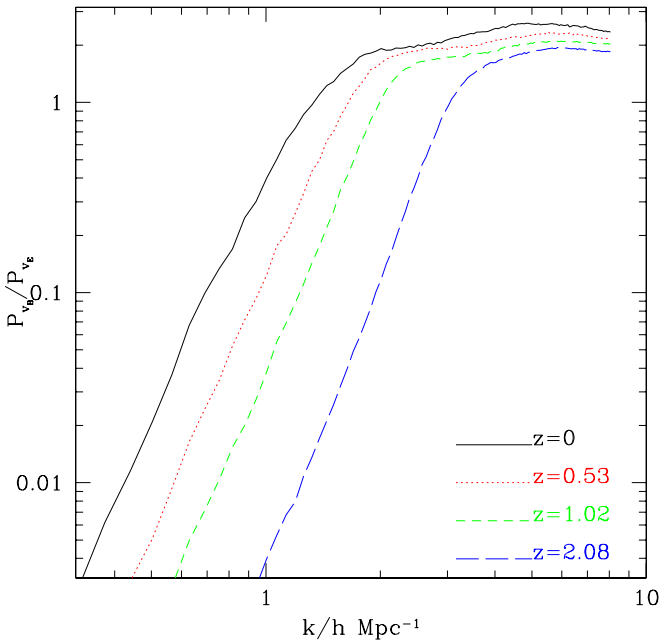

Figure B1. The ratio of the power spectra of E-mode velocity and B-mode velocity. The results are the ratios of total B-mode powers and E-mode powers, different from average method of other figures. $\mathbf{v}_B$ is comparable to $\mathbf{v}_E$ beyond $k \simeq 2h\,\mathrm{Mpc}^{-1}$ at $z = 0$, and this characteristic scale moves to smaller scales at higher redshifts as velocity is subject to less nonlinearities at early epochs.

APPENDIX B: THE INTERFERENCE OF THE "B"-MODE VELOCITY

Our velocity estimator (Eq. 3), by construction, can only recover the irrotational part of the velocity (the so called "E"-mode velocity, $\mathbf{v}_E$). Since "B"-mode velocity (rotational part of the velocity, $\mathbf{v}_B$) also contributes to the kSZ effect, missing $\mathbf{v}_B$ degrades the reconstruction and the kinetic SZ tomography. This is not a severe issue at large scales where $\mathbf{v}_B$ is negligible. However, at small scales multi-streaming develops and $\mathbf{v}_B$ begins to grow. Turbulence in the gas fluid, which can be amplified by gastrophysical processes like supernovae feedback, also contributes to $\mathbf{v}_B$. To better understand the impact of $\mathbf{v}_B$, we directly measure it from our simulations.

The E-B modes can be obtained straightforwardly in Fourier space by

$$\begin{aligned}\mathbf{v}_E(\mathbf{k}) &= \mathbf{v}_b(\mathbf{k})\cdot\hat{\mathbf{k}}\,,\\ \mathbf{v}_B(\mathbf{k}) &= \mathbf{v}_b(\mathbf{k}) - \mathbf{v}_E(\mathbf{k})\,.\end{aligned} \tag{B1}$$

The ratio of the two power spectra in our non-adiabatic run is shown in Fig. B1. As expected, the power spectrum of the "B"-mode velocity is much smaller than the "E"-mode velocity power spectrum on large scales. This is especially true at $z \gtrsim 1$ and $k \lesssim 1h$/Mpc. This is one of the major reasons for the reasonably good performance of the reconstruction at these scales and redshifts. The B-mode increases towards lower redshifts where the nonlinearities are stronger. At $z = 0$ and $k \gtrsim 1h\,\mathrm{Mpc}^{-1}$, it is already comparable to the E-mode. This behavior is largely responsible to poorer reconstruction at $k \gtrsim 1h\,\mathrm{Mpc}^{-1}$, especially in redshift space (refer to §3.2.2).

Velocity measurement can be tricky in simulations, due to numerical artifacts, sampling bias in the velocity assignment and

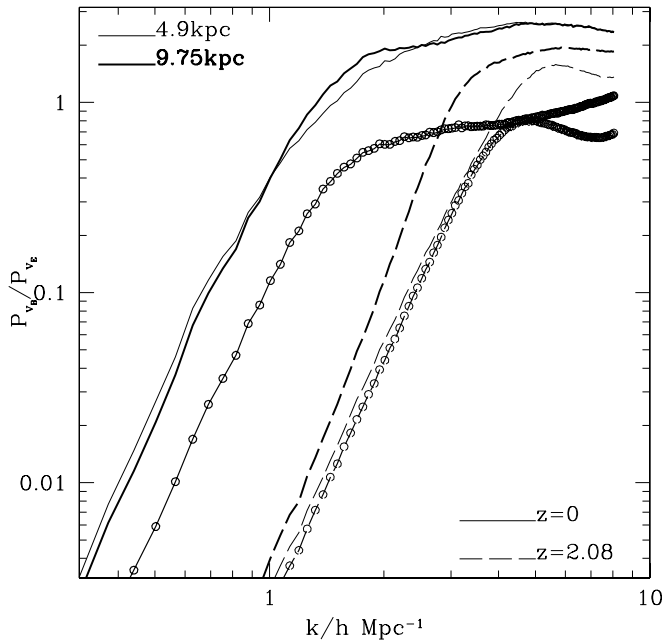

Figure B2. The comparison of the gas velocity power spectrum ratio $P_{\mathbf{v}_B}/P_{\mathbf{v}_E}$ in the non-adiabatic simulation (thick lines) and the adiabatic one (thin lines). Also shown are the ratios of dark matter velocity power spectrum ratio (lines for adiabatic, open circles for non-adiabatic). The two simulations have different softening length, with $9.75h^{-1}$ kpc (non-adiabatic) vs. $4.9h^{-1}$ kpc (adiabatic). The difference in softening length has virtually no impact on $P_{\mathbf{v}_B}/P_{\mathbf{v}_E}$ of dark matter. So the significant changes in the gas velocity power spectrum between two simulations is very likely caused by differences in the gastrophysics other than difference in the softening length. We need to model "B"-mode velocity carefully in the existence of these gastrophysical processes, an important ingredient in the kSZ effect modeling.

missing gastrophysics (e.g. Pueblas & Scoccimarro 2009). We do not attempt to perform a detailed study on these issues. Rather, we present a simple comparison between the two simulations available. The two simulations share the same initial conditions and the same cosmology parameters. However, the gravitational softening lengths are different. The one of the non-adiabatic run is $9.75h^{-1}$ kpc, twice as large as the adiabatic one, $4.9h^{-1}$ kpc. With the two simulations, we can perform interesting observations on the following issues:

- Difference between the velocity field of dark matter and that of gas. Understanding this difference helps improve models on the kSZ effect.
- The impact of gastrophysics on the gas velocity. Radiative and dynamical feedback can both cause turbulence in the gas fluid and thus affect the B-mode velocity. Comparing the gas velocity in the two simulations, we are able to get a handle on this issue.
- The impact of the simulation softening length. The two simulations have different softening length. Comparing the dark matter velocity in the two simulations, we can estimate its impact. The reason that we do not use gas velocity to do the comparison is that the gas velocity is also affected by different gastrophysics in the two simulations.

The ratios of two power spectra, $P_{\mathbf{v}_B}/P_{\mathbf{v}_E}$, are shown in Fig. B2. Since dark matter velocity is insensitive to gastrophysics, differences, if any, between the two simulations are likely caused by difference in the softening length. We find the dark matter velocity has virtually no change in the two simulations. So the influence of softening length to the dark matter velocity is negligible. Although we are not able to directly quantify the influence of softening length to the gas velocity, this result suggests that the influence of softening length should be also under control for the gas velocity.

To the opposite, the gas velocity differs significantly between the two simulations, reflecting the significant influence of gastrophysics. At $z = 2.08$, the B-mode velocity of the non-adiabatic run is a factor of a few larger than that of the adiabatic run, likely caused by strong star formation and supernovae feedback at that epoch. Interestingly, this amplification in the B-mode velocity by gastrophysics at $z = 2.08$ is significantly weakened or even altered at $z = 0$. This is likely correlated with the fact that star formation rate decreases significantly from $z = 2$ to $z = 0$.

The vorticity in the gas velocity is larger than that in the dark matter velocity at all redshifts, all scales and in both simulations. This difference is likely caused by gas viscosity and dissipation. It is an important issue to understand in order to improve the kSZ modeling.